ONLY

Mission Research Corporation

MRC/COS-R-894-SAN
Copy

[redacted] CWMS TEST DATA ANALYSIS REPORT, Sanitized Version

Wolfgang A. Bereuter
Robert A. Racca

7 March 1989

19981106 135

Prepared for: US Army Engineer Division, Huntsville
Contract # DACA87-88-C-0055
CDRL Item No. 0029, Test 1
Full Scale Test Program

Prepared by: MISSION RESEARCH CORPORATION
4935 North 30th Street
Colorado Springs, CO 80919

Views, opinions, and/or findings contained in the report are those of the author(s) and should not be construed as an official Department of the Army position, policy, or decision unless so designated by other documentation.

Sponsored by the Defense Nuclear Agency (DNA)
Monitored by the US Army Engineer Division, Huntsville

MRC/COS-R-894
Copy ____________

[redacted] CWMS TEST DATA ANALYSIS REPORT

Wolfgang A. Bereuter
Robert A. Racca

7 March 1989

Prepared for: US Army Engineer Division, Huntsville
Contract # DACA87-88-C-0055
CDRL Item No. 0029, Test 1
Full Scale Test Program

Prepared by: MISSION RESEARCH CORPORATION
4935 North 30th Street
Colorado Springs, CO 80919

Sponsored by the Defense Nuclear Agency (DNA)
Monitored by the US Army Engineer Division, Huntsville

SECURITY CLASSIFICATION OF THIS PAGE

Form Approved
OMB No. 0704-0188
Exp. Date: Jun 30, 1985

REPORT DOCUMENTATION PAGE

1a. REPORT SECURITY CLASSIFICATION
UNCLASSIFIED

1b. RESTRICTIVE MARKINGS
N/A Since Unclassified

2a. SECURITY CLASSIFICATION AUTHORITY
N/A Since Unclassified

3. DISTRIBUTION/AVAILABILITY OF REPORT
Reproduction requires approval of originator or higher DoD Authority. Further dissemination only as directed by DNA or higher

2b. DECLASSIFICATION/DOWNGRADING SCHEDULE
N/A Since Unclassified

4. PERFORMING ORGANIZATION REPORT NUMBER(S)
MRC/COS-R-894

5. MONITORING ORGANIZATION REPORT NUMBER(S)

6a. NAME OF PERFORMING ORGANIZATION
Mission Research Corporation

6b. OFFICE SYMBOL *(If applicable)*

7a. NAME OF MONITORING ORGANIZATION
US Army Engineer Division, Huntsville

6c. ADDRESS *(City, State, and ZIP code)*
4935 North 30th Street
Colorado Springs, CO
80919

7b. ADDRESS *(City, State, and ZIP code)*
PO Box 1600 (106 Wynn Drive)
Huntsville, AL
35807-4301

8a. NAME OF FUNDING/SPONSORING ORGANIZATION
Defense Nuclear Agency

8b. OFFICE SYMBOL *(If applicable)*

9. PROCUREMENT INSTRUMENT IDENTIFICATION NO.
DACA87-88-C-0055

8c. ADDRESS *(City, State, and ZIP code)*
6801 Telegraph Road
Alexandria, VA 22310

10. SOURCE OF FUNDING NUMBERS

PROGRAM ELEMENT NO.	PROJECT NO.	TASK NO.	WORK UNIT ACCESSION NO

11. TITLE *(Include Security Classification)*
[redacted] CWMS TEST DATA ANALYSIS REPORT

12. PERSONAL AUTHOR(S)
Bereuter, W. A., Racca, R. A.

13a. TYPE OF REPORT
Final

13b. TIME COVERED
From 881101 To 890228

14. Date of Report *(Year, Month, Day)*
890207

15. PAGE COUNT
80

16. SUPPLEMENTARY NOTATION

17. COSATI CODES

FIELD	GROUP	SUB-GROUP

18. SUBJECT TERMS *(continue on reverse if necessary and identify by block number)*
HEMP, Continous Wave Measurement System (CWMS), [redacted] HAVSTAP

19. ABSTRACT *(Continue on reverse if necessary and identify by block number)*

This report documents the results of the CW Illumination and Direct Drive Test [redacted]. The test was performed by the HAVSTAP in support of the Harry Diamond Laboratories HEMP Hardness verification program.

20. DISTRIBUTION AVAILABILITY OF ABSTRACT
☐ Unclassified/Unlimited ☐ Same as RPT. ☐ DTIC Users

21. ABSTRACT SECURITY CLASSIFICATION
UNCLASSIFIED

22a. NAME OF RESPONSIBLE INDIVIDUAL

22b. TELEPHONE *(Include Area Code)*

22c. OFFICE SYMBOL

DD FORM 1473, 84 MAR — 83 Apr edition may be used until exhausted. All other editions are obsolete

SECURITY CLASSIFICATION THIS PAGE
UNCLASSIFIED

SECURITY CLASSIFICATION OF THIS PAGE

"WARNING - This document contains technical data whose export is restricted by the Arms Export Control Act (Title 22, U.S.C., Sec. 2751 et seq.) or Executive Order 12470. Violation of these export laws are subject to severe criminal penalties."

"DESTRUCTION NOTICE - For classified documents, follow the procedures in DoD 5200.22-M, Industrial Security Manual, Section II-19 or DoD 5200.1-R, Information Security Program Regulations, Chapter IX. For unclassified, limited documents, destroy by any method that will prevent disclosure of contents or reconstruction of the documents."

SECURITY CLASSIFICATION THIS PAGE

UNCLASSIFIED

PREFACE

The Hardness Verification/Surveillance Testing and Standards Program (HAVSTAP) is funded by the Defense Nuclear Agency (DNA) and other government agencies through the Corps of Engineers (CoE) U.S. Army Engineer Division Huntsville (US-AEDH). The contract monitor for the CoE is Mr. John Loyd, and the DNA technical monitor is Mr. Sam Mauch.

Mission Research Corporation (MRC) is the prime contractor for the HAVSTAP, and IRT Corporation and Booz·Allen and Hamilton Inc. are subcontractors to MRC. Personnel from all three companies were instrumental in th[redacted] test.

Conversion Table

Conversion factors for U.S. Customary to metric (SI) units of measurement

MULTIPLY → BY → TO GET
TO GET ← BY ← DIVIDE

angstrom	1.000 000 X E -10	meters (m)
atmosphere (normal)	1.013 25 X E +2	kilo pascal (kPa)
bar	1.000 000 X E +2	kilo pascal (kPa)
barn	1.000 000 X E -28	meter^2 (m^2)
British thermal unit (thermochemical)	1.054 350 X E +3	joule (J)
calorie (thermochemical)	4.184 000	joule (J)
cal (thermochemical)/cm^2	4.184 000 X E -2	mega joule/m^2 (MJ/m^2)
curie	3.700 000 X E +1	*giga becquerel (GBq)
degree (angle)	1.745 329 X E -2	radian (rad)
degree Fahrenheit	$T_K = (T°F + 459.67)/1.8$	degree kelvin (K)
electron volt	1.602 19 X E -19	joule (J)
erg	1.000 000 X E -7	joule (J)
erg/second	1.000 000 X E -7	watt (W)
foot	3.048 000 X E -1	meter (m)
foot-pound-force	1.355 818	joule (J)
gallon (U.S. liquid)	3.785 412 X E -3	meter^3 (m^3)
inch	2.540 000 X E -2	meter (m)
jerk	1.000 000 X E +9	joule (J)
joule/kilogram (J/kg) (radiation dose absorbed)	1.000 000	Gray (Gy)
kilotons	4.183	terajoules
kip (1000 lbf)	4.448 222 X E +3	newton (N)
kip/inch^2 (ksi)	6.894 757 X E +3	kilo pascal (kPa)
ktsp	1.000 000 X E +2	newton-second/m^2 (N-s/m^2)
micron	1.000 000 X E -6	meter (m)
mil	2.540 000 X E -5	meter (m)
mile (international)	1.609 344 X E +3	meter (m)
ounce	2.834 952 X E -2	kilogram (kg)
pound-force (lbs avoirdupois)	4.448 222	newton (N)
pound-force inch	1.129 848 X E -1	newton-meter (N·m)
pound-force/inch	1.751 268 X E +2	newton/meter (N/m)
pound-force/foot^2	4.786 026 X E -2	kilo pascal (kPa)
pound-force/inch^2 (psi)	6.894 757	kilo pascal (kPa)
pound-mass (lbm avoirdupois)	4.535 924 X E -1	kilogram (kg)
pound-mass-foot^2 (moment of inertia)	4.214 011 X E -2	kilogram-meter^2 (kg·m^2)
pound-mass/foot^3	1.601 846 X E +1	kilogram/meter^3 (kg/m^3)
rad (radiation dose absorbed)	1.000 000 X E -2	**Gray (Gy)
roentgen	2.579 760 X E -4	coulomb/kilogram (C/kg)
shake	1.000 000 X E -8	second (s)
slug	1.459 390 X E +1	kilogram (kg)
torr (mm Hg, 0° C)	1.333 22 X E -1	kilo pascal (kPa)

* The becquerel (Bq) is the SI unit of radioactivity; 1 Bq = 1 event/s.

** The Gray (Gy) is the SI unit of absorbed radiation.

TABLE OF CONTENTS

LIST OF ILLUSTRATIONS

Figure

Figure **Page**

LIST OF TABLES

SECTION 1

INTRODUCTION

1.1 BACKGROUND

[redacted]

The Harry Diamond Laboratories (HDL) is conducting a HEMP hardness verification program [redacted] As part of this program, MIL-STD-285 shielding effectiveness tests were performed, and the conducted penetrations [redacted] were direct driven with high level pulses. For more information on the HDL effort see Reference 2.

To augment the HDL tests, the Defense Nuclear Agency (DNA) sponsored a low level CW test [redacted] The CW test was conducted from 26 September to 21 October 1988 to determine the HEMP induced stresses. The measurements were acquired with the DNA CWMS III (Continuous Wave Measurement System III). This test was performed under the auspices of the Hardness Verification/Surveillance

page 2 deleted in its entirety.

Testing and Standards Program (HAVSTAP). The test execution and lessons learned are documented in the Test Director's Report (Reference 1). The purpose of this report is to describe the data processing and to analyze the results.

1.2 TEST OBJECTIVES

The specific objectives of the CWMS tes[redacted]

1. Acquire HEMP stress estimates at internal equipment interfaces.

2. Determine the dominant source for these stresses.

3. Complement the DNA HEMP stress data base for Ground Based C^3I facilities with stress data from a well shielded facility.

4. Demonstrate the utility of CWMS testing for well shielded facilities.

[redacted]

6. Provide recommendations for additional testing to support the HDL hardness verification statement.

To meet these objectives, CW illumination and CW direct drive tests on the conducted penetrations were performed. Table 1 provides an overview of the number of test points monitored during the various elements of the test. CW illumination is discussed in Section 2, the single line direct drive data are described in Section 3, and bulk direct drive results are contained in Reference 3.

Table 1. Number of test locations for illumination, single line direct drive, and bulk direct drive tests.

CW ILLUMINATION [redacted]								
	[redacted]							
External Field Map							3	
External Cable Currents				9	7		9	
Internal Field Map	1	2	1					
Internal Cable Currents	41	19	2					5

CW SINGLE LINE DIRECT DRIVE	
[redacted]	58
	10
	8
	6
	8

CW BULK DIRECT DRIVE [redacted]	
[redacted]	25
	20
	32

Page 5 deleted in its entirety.

Other results:

[redacted]

(b) Valuable lessons were learned in HEMP testing and analysis.

SECTION 2

ILLUMINATION MEASUREMENTS

2.1 EXTRAPOLATION

The illumination test was performed with the CWMS inverted-V antenna. Due to the uneven terrain and the security fence around the property there were only few options for installing the antenna. Figure 2 shows the antenna location for the CW illumination test at the ETC. The inverted-V antenna simulates a horizontally polarized incident plane wave with elevation angle roughly 34° with field components E_y, H_x, and H_z.

Figure 2 also shows the location of the reference sensor (on the antenna center line, 20 m south of the antenna, 1 m above ground). The reference sensor measures the total H_x field produced by the radiating antenna. The reason for this particular placement of the reference sensor is to minimize undesirable scattering off the building. Thus the reference sensor is placed on the opposite side of the antenna utilizing the field symmetry (with respect to the y-axis) properties of the antenna.

The field measured by the reference sensor is identical to the field which would be at the symmetrical location (i.e., [redacted] in the absence of the building.

CWMS III measures the current induced on cables, relative to the simulation field at the reference sensor. Mathematically each measurement is a transfer function of the form:

$$\left(\frac{TP}{H_x(R)}\right)_{ill} \qquad \frac{A}{A/m} \tag{1}$$

where TP represents the test signal induced on the cable measured, $H_x(R)$ is the x-component of the magnetic field measured at the reference sensor, and the subscript "ill" denotes an illumination measurement.

To obtain an estimate of the HEMP induced current, the transfer function must be multiplied by the total (incident plus ground reflected) HEMP field at the reference sensor location. Specifically, this field is the total H_x which would exist at the

Pg 8 deleted in its entirety.

reference sensor location in an actual HEMP event. The total H_x is calculated using a 34° angle of incidence, and with the following soil parameters: relative permittivity $\epsilon/\epsilon_0 = 10$, and conductivity $\sigma = 4$ mmho/m.

Since the simulation fields satisfy Maxwell's equations, the other field components are automatically scaled to the appropriate HEMP environment.

The incident HEMP waveform is the double exponential waveform

$$E^{inc}(t) = E_0(e^{-\alpha t} - e^{-\beta t}) \qquad (V/m) \tag{2}$$

in Figure 3, where also the values for the parameters are provided. The relationship of this waveform with other HEMP environments is discussed in Reference 4. The corresponding magnetic field is

$$H^{inc} = E^{inc}/376.7 \qquad (A/m) \tag{3}$$

and the magnetic field component in the x-direction is

$$H_x^{inc} = H^{inc} cos(34°) \qquad (A/m). \tag{4}$$

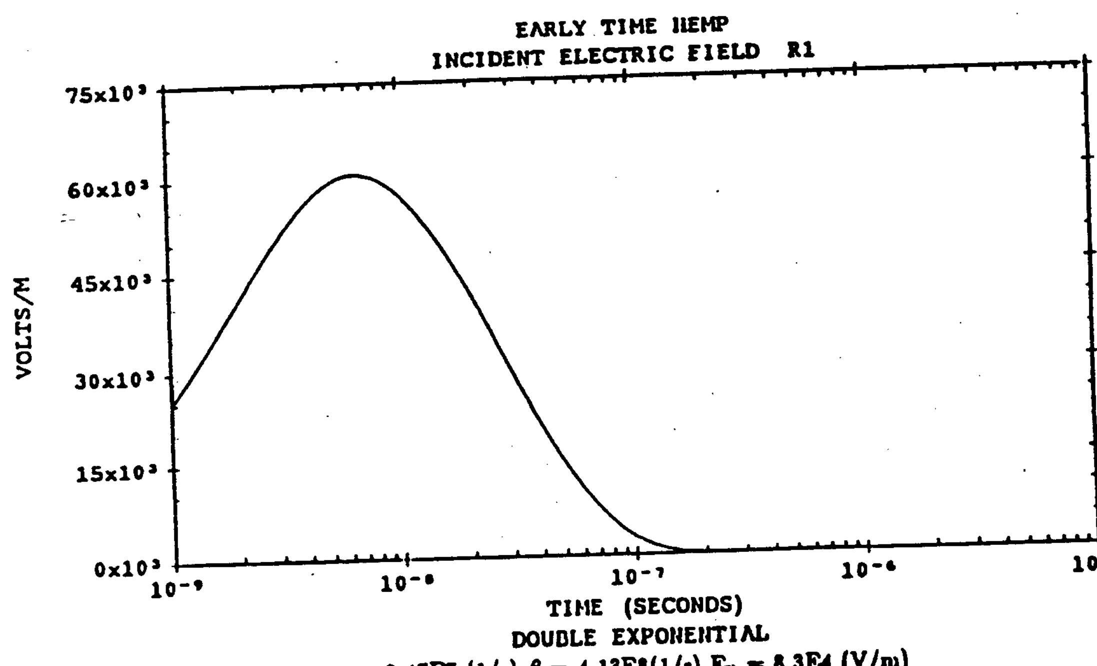

Figure 3. Incident HEMP electric field double exponential waveform.

Figure 4 shows H_z^{inc}, and the corresponding total H_z^{tot}, which was used to extrapolate all illumination test measurements to HEMP.

Butterworth Band Pass Filter: The extrapolation is performed in the frequency domain. To obtain time domain transients, the frequency spectra must be inverse Fourier transformed. CWMS illumination measurements are acquired from 100 kHz to 100 MHz, thus the extrapolated spectra are band limited to this range. This limitation is imposed by the usable frequency range of the simulator antenna, and a justification for this frequency range is beyond the scope of this report (e.g., Reference 5). The practical consequence of this limitation is that the quality of inverse Fourier transforms can suffer due to the abrupt transition of the spectra to zero at 100 kHz and 100 MHz. To smooth the transition at the ends of the measurement band, a Butterworth Filter (pass band 200 kHz to 80 MHz) is used on all cable current measurements. (Therefore, Fourier transforms are carried out to 5 μs.) The product of the Butterworth Filter characteristic with the HEMP H_z^{tot} from Figure 4 is shown in Figure 5.

Thus the formula for extrapolating illumination measurements is:

$$I^{thr}(f) = \left(\frac{TP}{H_z(R)}\right)_{ill} \cdot H_z^{thr}(f) \quad (A/Hz) \tag{5}$$

where TP indicates the test point measured, $H_z(R)$ is the simulation field measured by the reference sensor, and H_z^{thr} is as in Figure 5.

Simulation Error: The incident HEMP is specified as a plane wave. However, the inverted-V antenna can only approximate a plane wave. The extrapolation numerically simulates exactly the specified HEMP environment at the reference sensor, and also at the corresponding locatio[redacted](due to the field symmetry with respect to the y-axis). At all other locations, the simulated fields only approximate the specified HEMP environment. The accuracy of the approximation was investigated in References 6 and 7. [redacted]

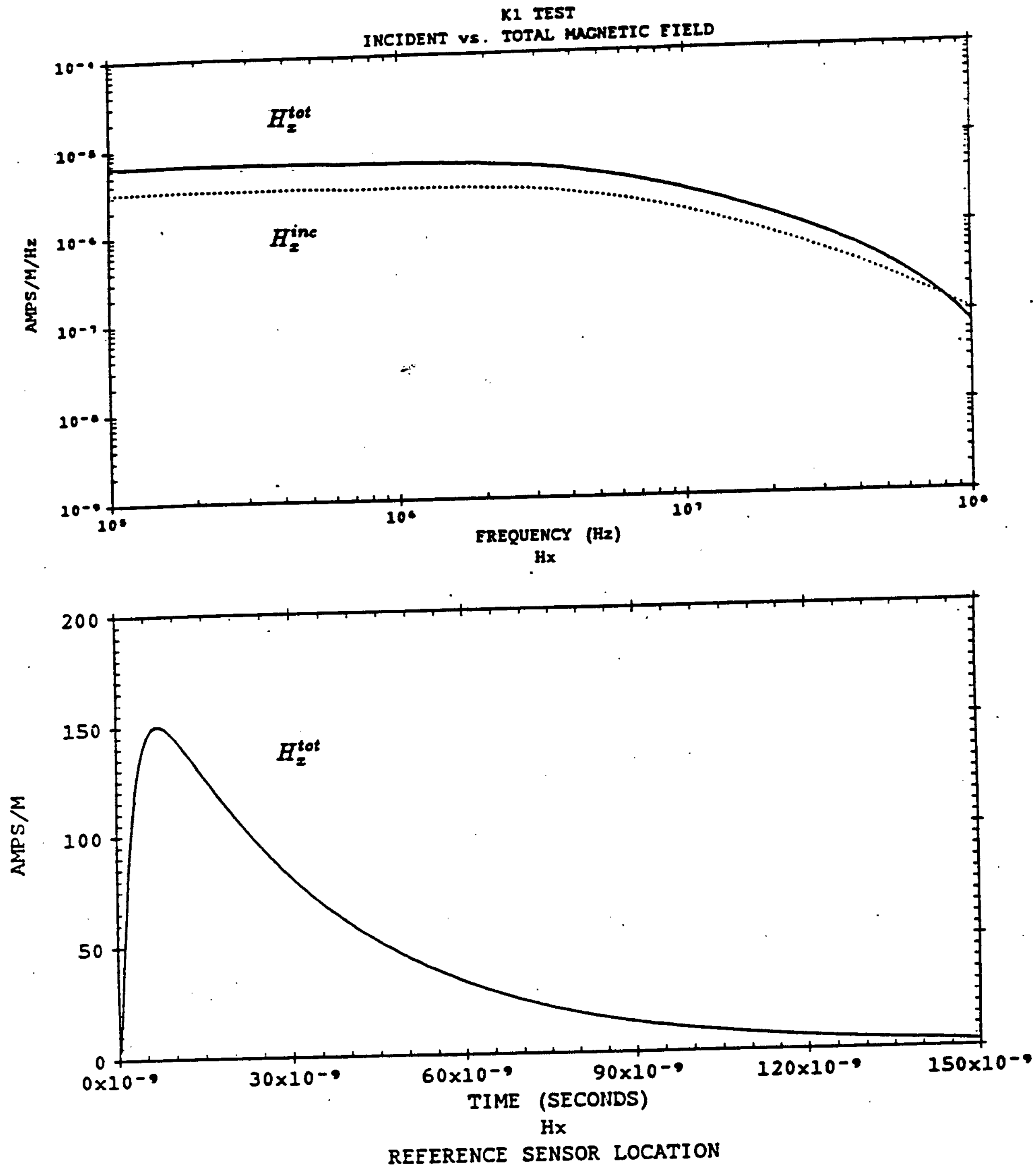

Figure 4. **Incident HEMP H_z^{inc} vs. total HEMP H_z^{tot} spectra, and total HEMP H_z^{tot} time waveform.**

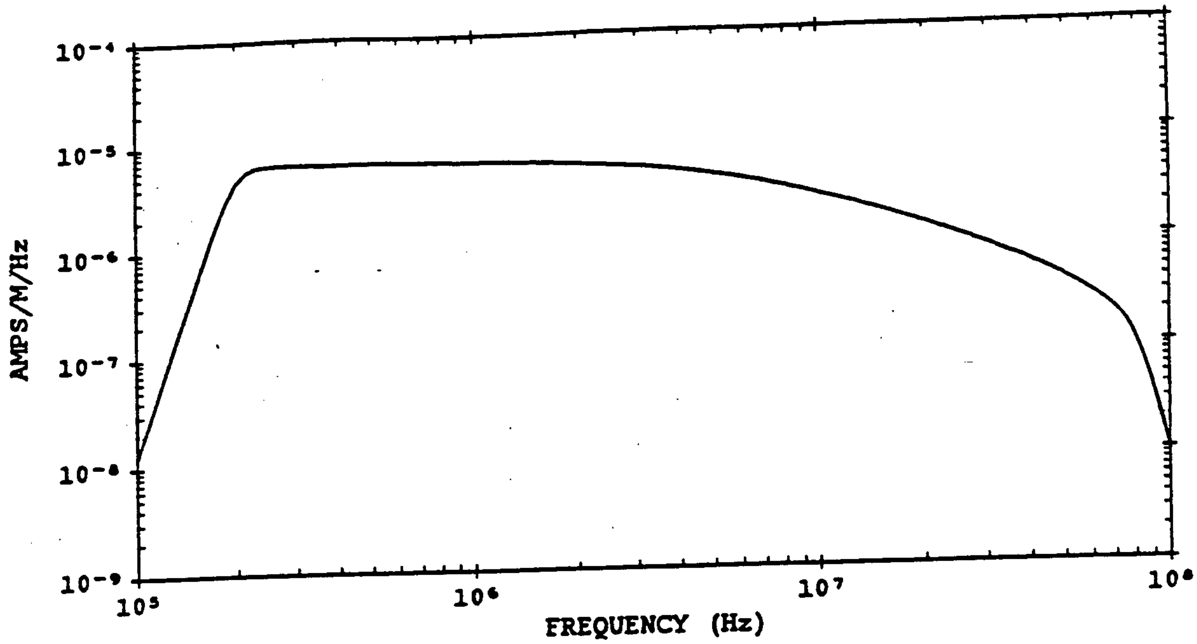

Figure 5. **Extrapolation function H_z^{thr} including Butterworth Filter for cable current transfer functions.**

2.2 EXTERNAL MEASUREMENTS

2.2.1 EXTERNAL FIELD MAP

The purpose of the field map at the external locations FM1, FM2, and [redacted] is to provide data on the non-uniformity of the simulation field along th[redacted] CWMS measures field transfer functions analogous to cable current transfer functions. In other words, just like cable measurements, fields are also measured relative to the $H_z(R)$ measured at the reference sensor. Therefore, to extrapolate field transfer functions to HEMP, the measurements are multiplied by HEMP H_z^{tot} shown in Figure 4. (The Butterworth Filter is not necessary for field measurements because their low frequency content is small, and at the high frequency end the rolloff of the HEMP spectrum automatically provides a sufficiently smooth transition.)

Figure 6 shows the extrapolated field measurements. Ideally the field at the three field map locations would be identical to the field transient at the reference sensor shown in Figure 4.

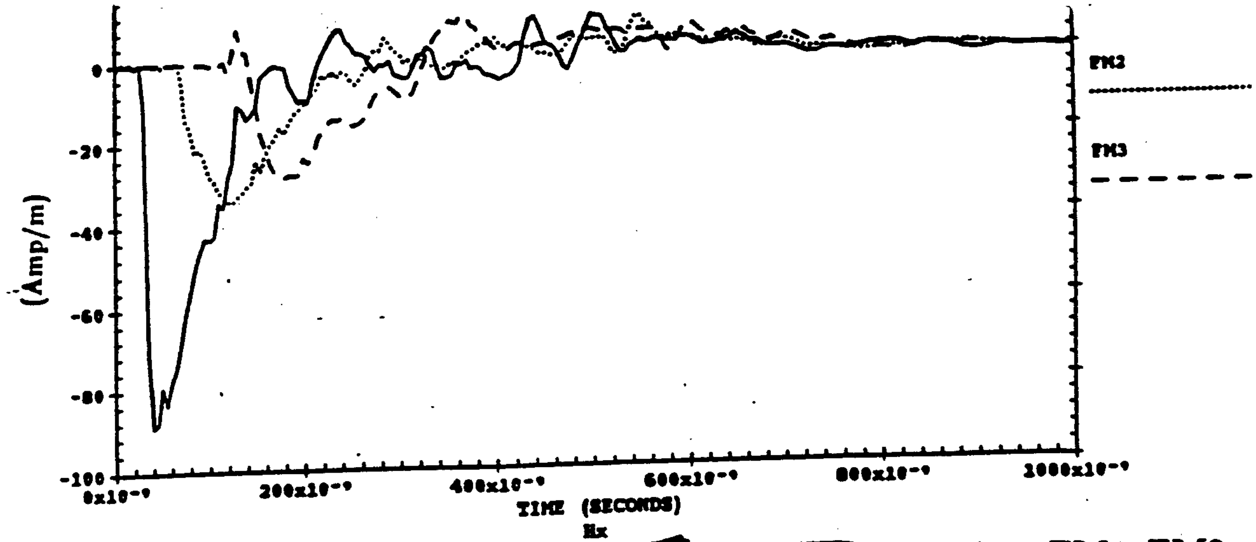

Figure 6. **Extrapolated H_z at [redacted] locations FM1, FM2, and FM3.**

However, it is evident from Figure 6 that the simulation field decreases as one moves away from the antenna centerline (x-axis). In other words, the peak H_z field [redacted] is lower than the field at the reference sensor (150 A/m), and decreases from 89.0 A/m at FM1 to 29.1 A/m at FM3. Also the field pulses are delayed in time (t = 0 when the field arrives at the reference sensor) due to the differences in propagation length to the three locations. (The high frequency components emanate from the bicone at the center of the inverted-V antenna.)

Consequently the currents induced on th[redacted] in the illumination test are not equal to those which would be induced by a HEMP plane wave. To bound this illumination deficiency, the field measurements [redacted] are averaged as follows:

$$\mathrm{AVE}(f) = \frac{1}{3}\left[\frac{H_z(FM1)}{H_z(R)} + \frac{H_z(FM2)}{H_z(R)} + \frac{H_z(FM3)}{H_z(R)}\right] \qquad (6)$$

AVE is the average simulation H_z along th[redacted] relative to the H_z at the reference sensor, i.e., AVE is the average illumination deficiency. AVE would be equal to unity at all frequencies if the simulated field were a uniform plane wave. The reciprocal of AVE quantifies the simulation field deficiencies, i.e., the correction function to compensate for the deficiencies is given by:

$$CORR(f) = 1/\mathrm{AVE}(f) \qquad (7)$$

The magnitude of this correction function is shown in Figure 7. Note that at frequencies below 1 MHz the deficiency is only on the order of 4 dB, but above 10 MHz the error is greater than 10 dB and rapidly varying with frequency. The reason for the spiky behavior is that AVE is the sum of three complex spectra which are Fourier transforms of delayed transients (cf. Figure 6). The effect of the time delays between the three transients is that at every frequency their phases either combine constructively (creating a peak), or destructively (producing a null).

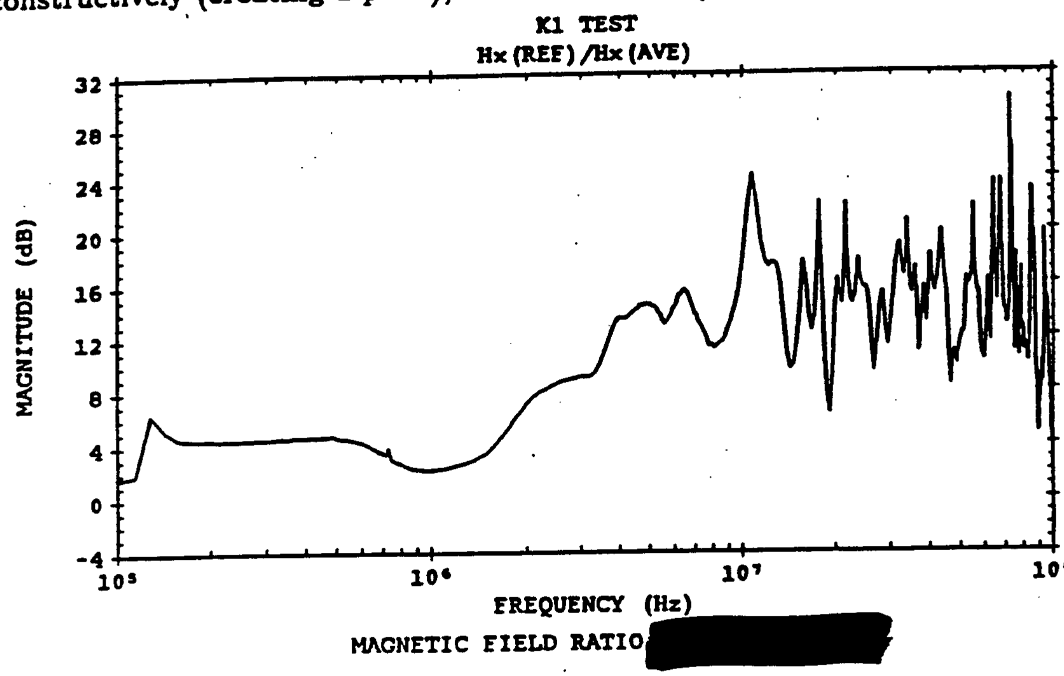

Figure 7. Magnitude of the correction function CORR(f).

An error bound for the illumination deficiency will be obtained by multiplying th[redacted] current measurements by CORR(f). Since CORR(f) is the reciprocal of the average field[redacted], it will overcompensate for the illumination deficiency [redacted] (at FM1), it will result in the correct HEMP fields near the middle [redacted] (FM2), and it will undercompensate near the dish antenna (FM3).

Since the[redacted] were measured at th[redacted] CORR(f) will result in a conservative error bound.

2.2.2 [redacted]

This section discusses the currents measured on th[redacted] in the CW illumination test. [redacted]

[redacted]

The cable current measurements were made on the dirty side of the building shield (in the doghouses). The waveform norms for these currents are contained in Appendix A.

[redacted]

These measurements were extrapolated using the extrapolation function in Figure 5. The results are shown in Figure 9.

Note that the peak currents differ considerably among [redacted] cables [redacted]

Page 16 deleted in its entirety.

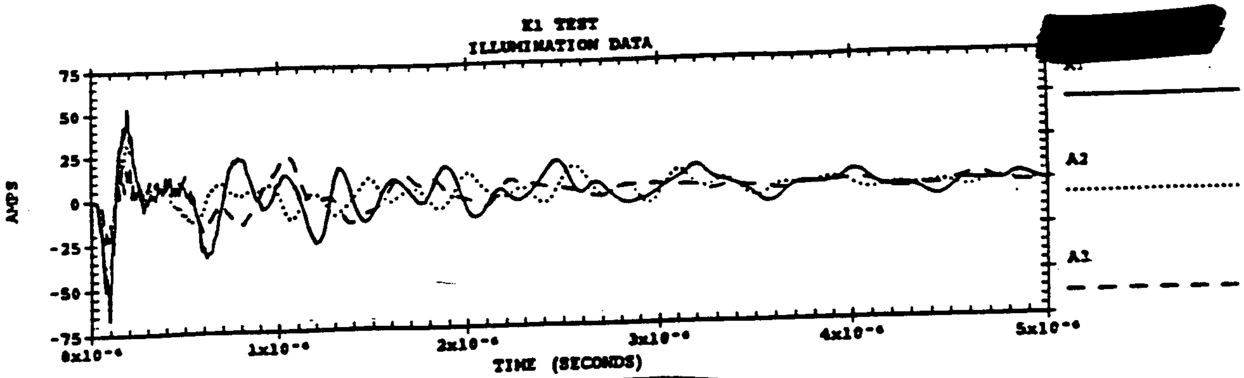

[redacted]

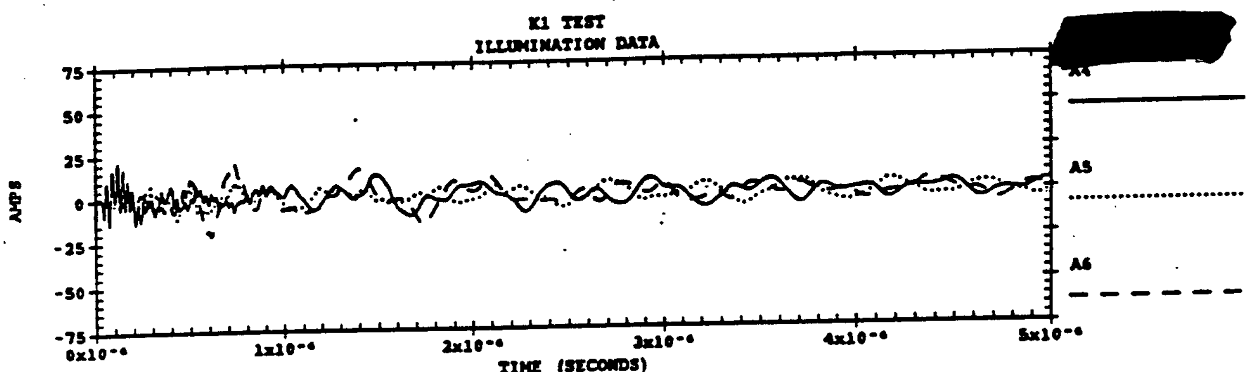

[redacted]

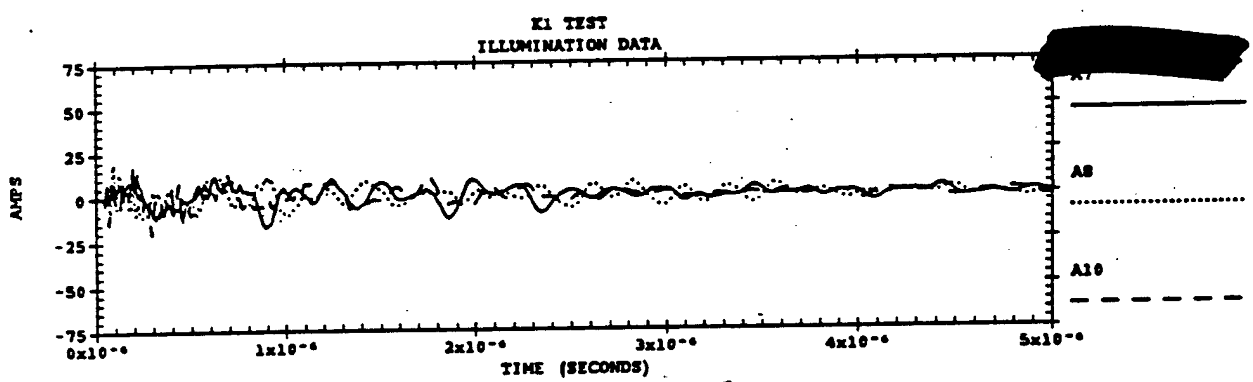

[redacted]

[redacted]

[redacted]

Error Bound: The results in Figure 9 are due to the simulation field which is not uniform as discussed in Section 2.2. To estimate the error due to this simulation deficiency, the extrapolate[redacted]measurements must be multiplied by the correction function CORR(f).

The resulting tota[redacted] current (I_{EAST}^{bound}) is shown in Figure 10. The correction factor CORR(f) significantly enhances the high frequency content[redacted]

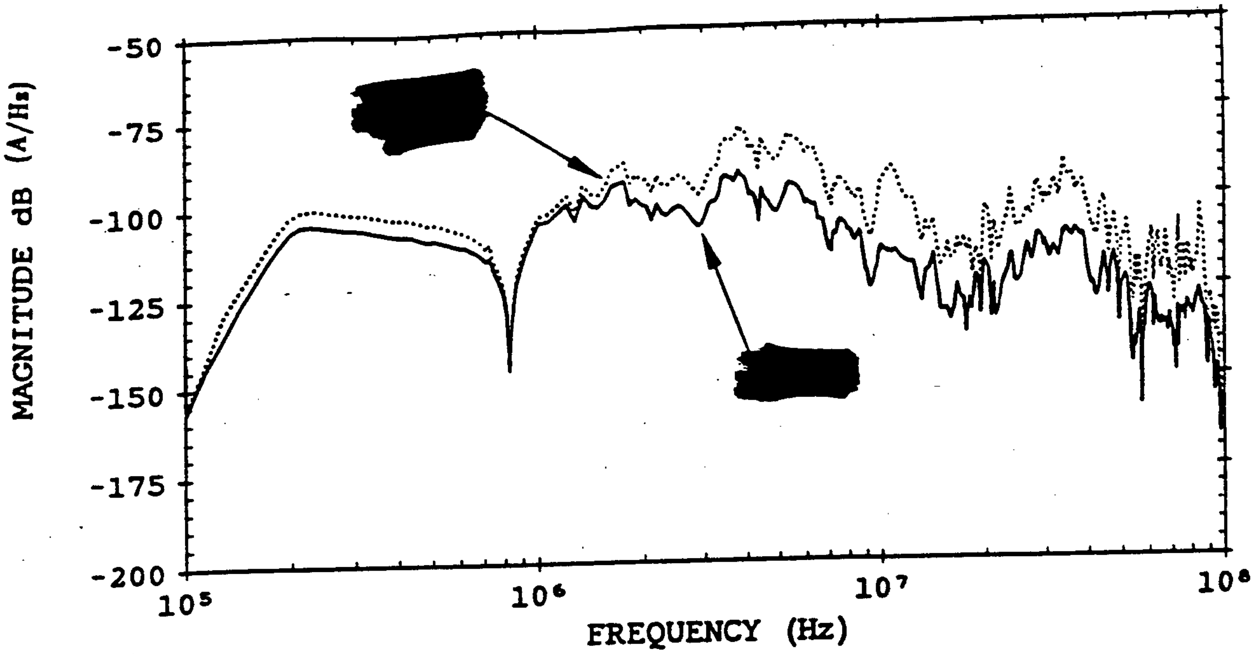

K1 TEST

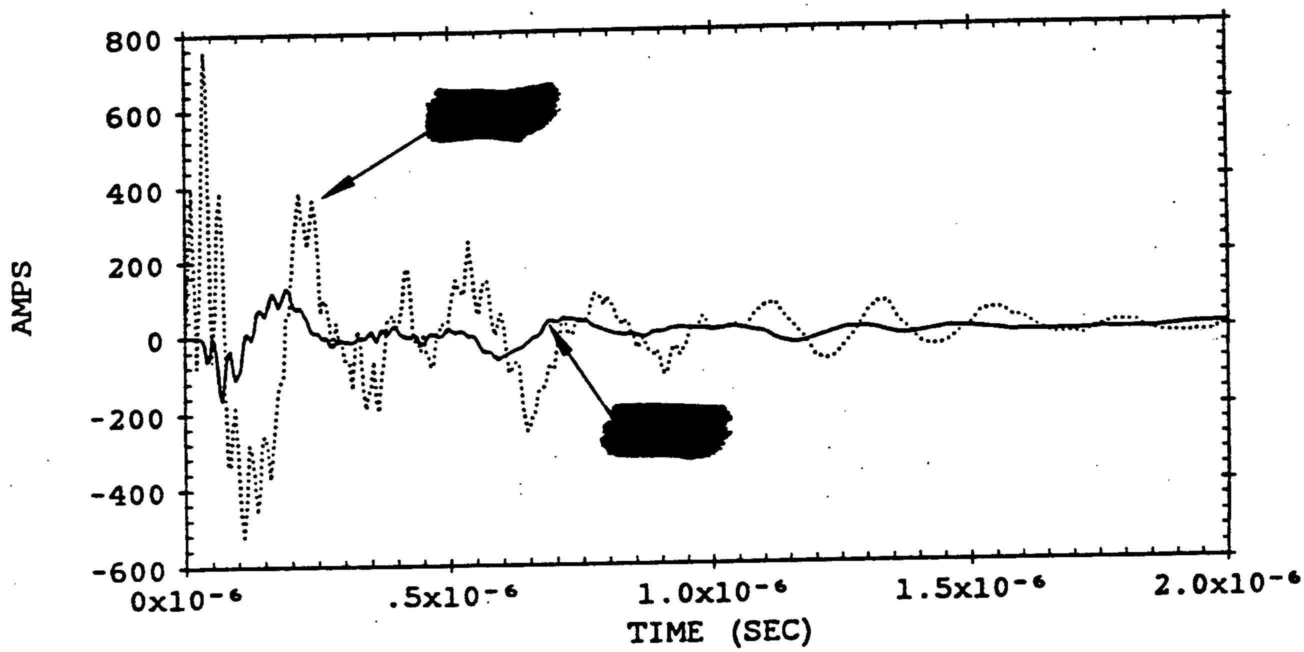

[redacted]

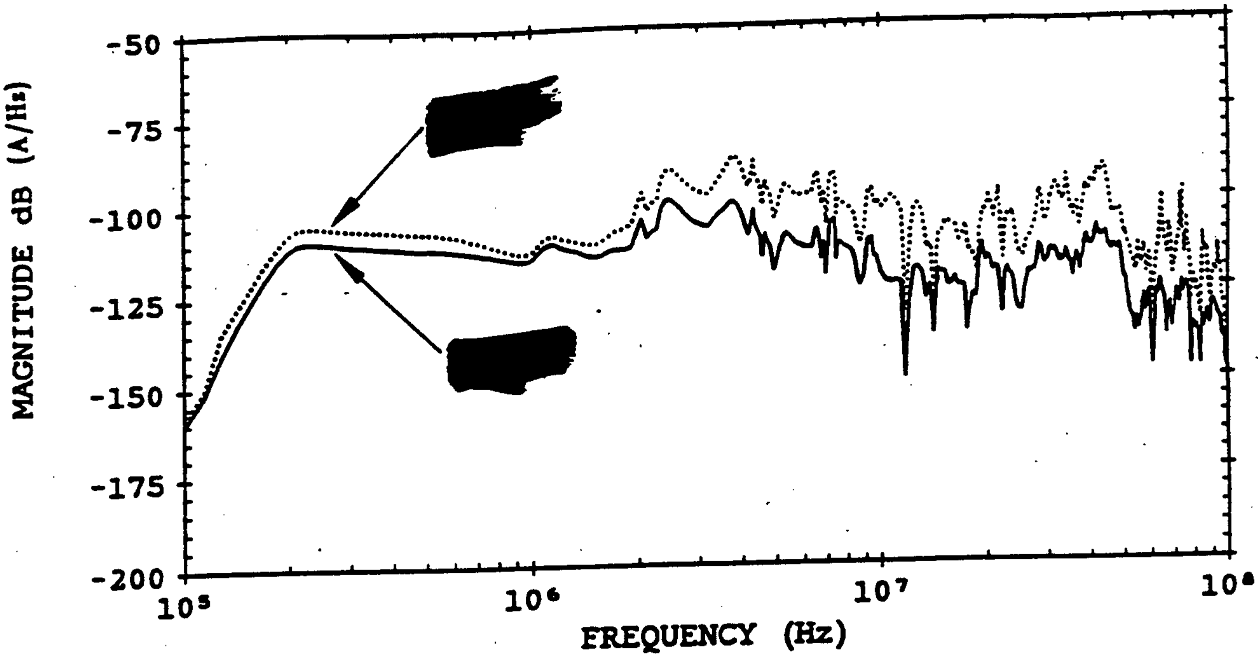

K1 TEST

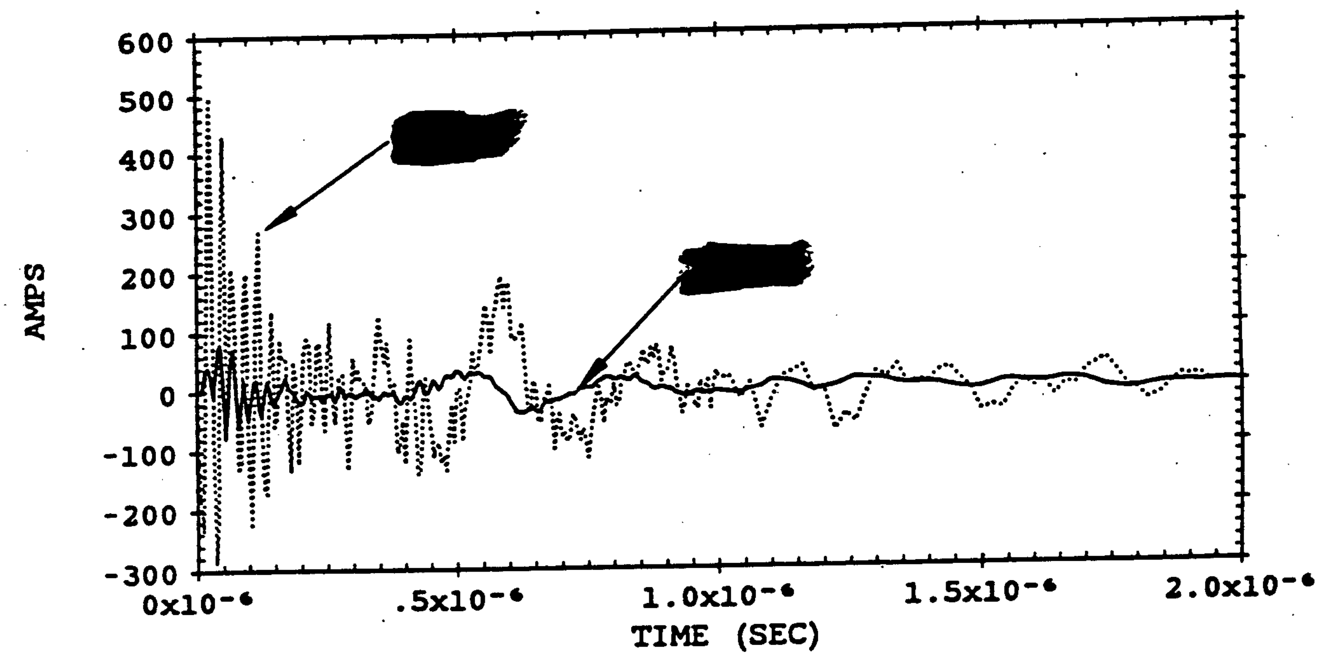

[redacted]

[redacted]

Figure 12 shows the total current [redacted] The currents induced [redacted] are highe[redacted] than expected. Although the currents measured on the [redacted] are probably not very accurate estimates of the actual currents induced by a HEMP, there are no data to bound the error. This is further discussed in Section 2.3.1.3.

2.3 INTERNAL MEASUREMENTS

The illumination measurements [redacted] rents inside [redacted]

In addition, internal field measurements were taken at two location[redacted]

2.3.1 INTERNAL CABLE CURRENT MEASUREMENTS

The purpose of the illumination cable current measurements is to dete[redacted] HEMP stresses at internal [redacted]. These internal [redacted] currents conducte[redacted]

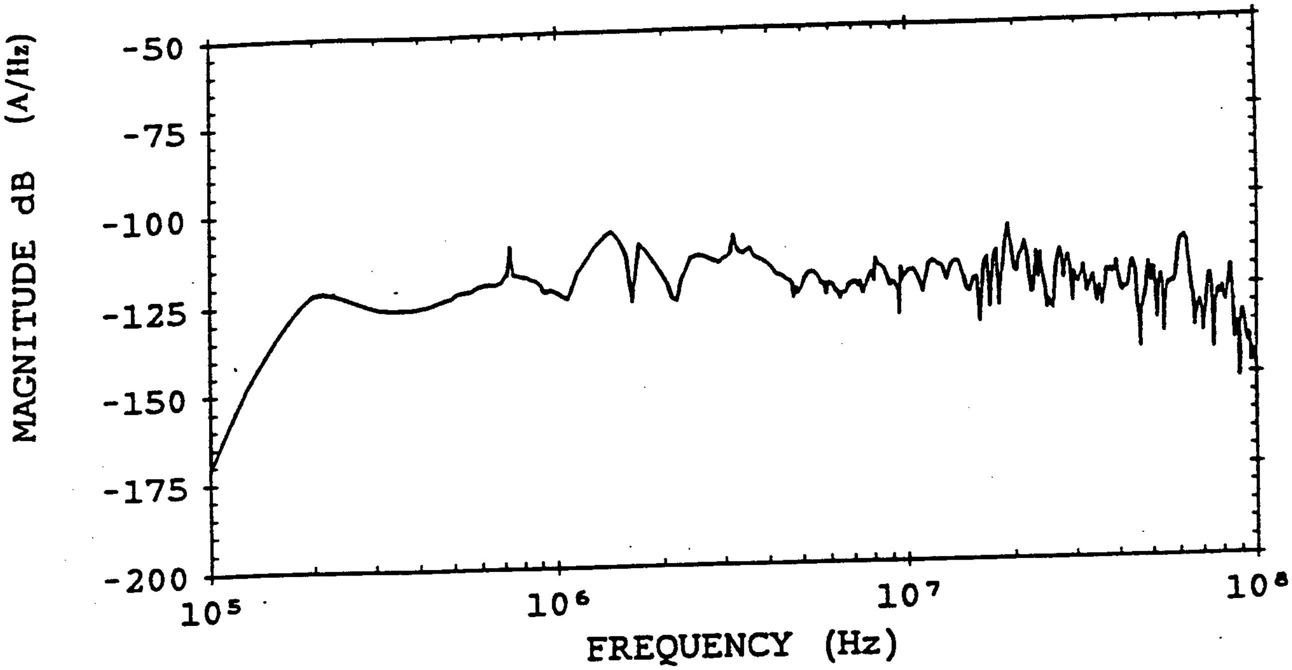

K1 TEST

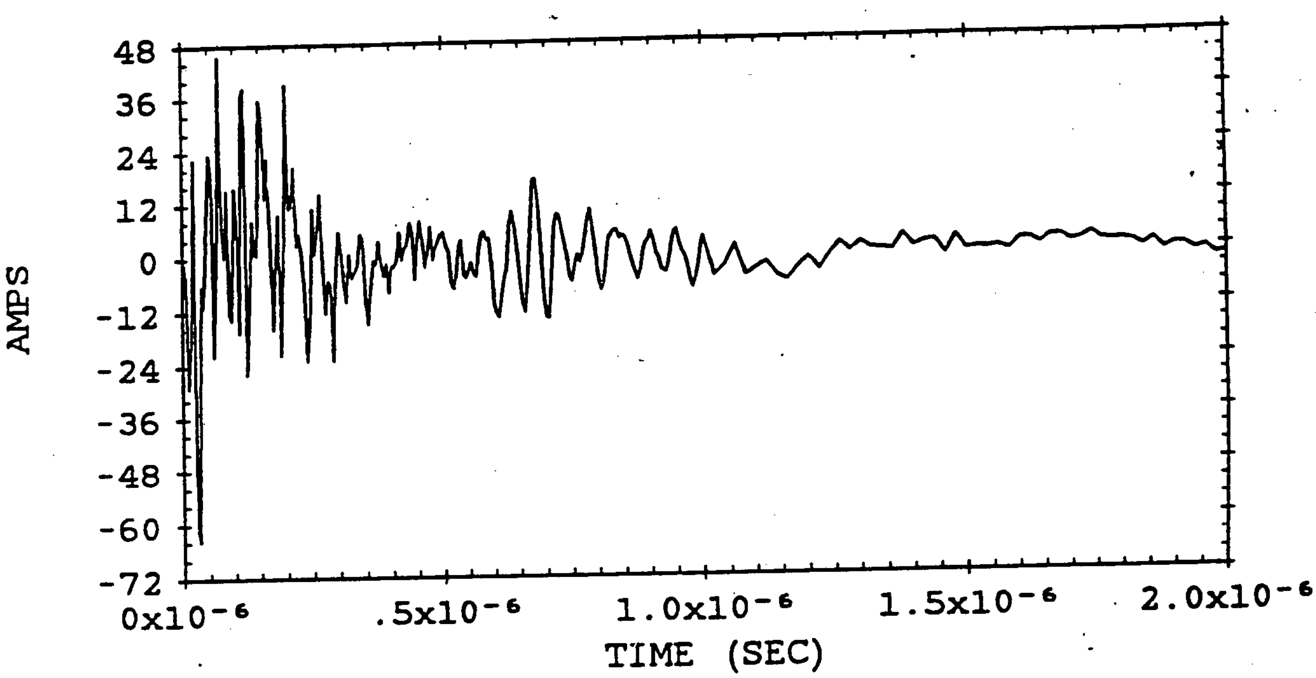

[redacted]

Test points labeled "B" are located [redacted] test points labeled "G" are [redacted], and test points labeled [redacted]. Test points are bundles of shielded and unshielded cables and wire bundles. Current measurements on single wires are generally impractical at operating facilities because they are often not accessible and because the CWMS test signals are usually dominated by the operating signal, which constitutes noise to CWMS measurements. Moreover it is impossible to survey complex communications facilities on the basis of single wire currents.

In the following the quality of the measurements is discussed, the HEMP stress estimates are presented, and the error due to the [redacted] illumination deficiency described in Section 2.2.2 is estimated. [redacted]

2.3.1.1 DATA QUALITY *S/N* Ratio: Since the ETC was operating throughout the CWMS test, the operating currents on the cables measured were competing with the CWMS induced test signal. Therefore, at every internal test point the facility generated ambient noise was measured (with the CWMS antenna muted), and compared with the CWMS signal at the test point. This Signal-to-Noise (S/N) relation is a comparison of the current detected in the signal (S) channel of the network analyzer due to CWMS illumination, and then due to the ambient noise (N). Note that S is not a CWMS transfer function, but is the numerator of the transfer function (the units of S and N are $A/\sqrt{Hz}$).

Figure 13 shows typical examples of the signals and noise at test points [redacted]. (Strictly speaking, the quantities compared are noise, and signal plus noise because the noise is always present.) The Signal- to-Noise ratio (in dB) is obtained by subtracting the dotted line (Noise in dB) from the solid line (Signal in dB) in Figure 13. However, instead of plotting this S/N ratio vs. frequency, it more illustrative to compare S and N directly as shown. With this illustration, for example, it can be observed how the noise "bites" the signal at isolated frequencies, and thus creates spikes in the transfer function.

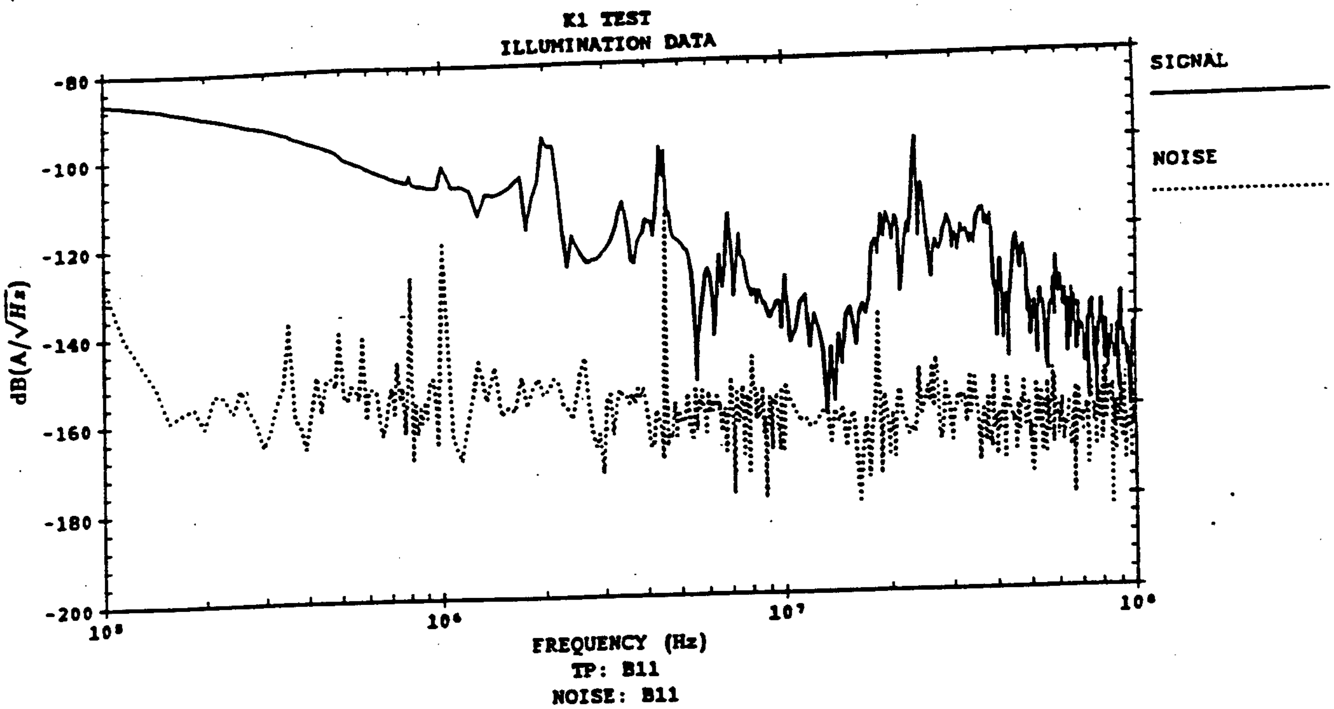

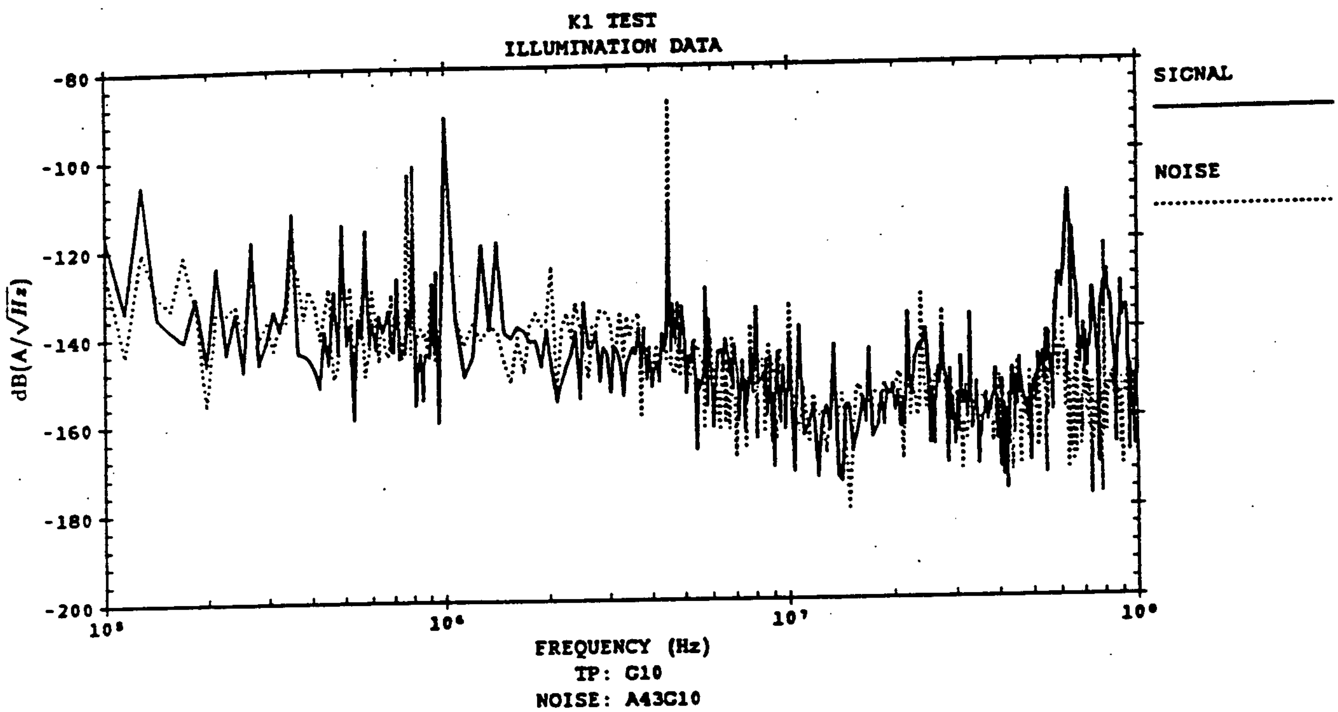

Figure 13. Signal and noise examples at test points [redacted] (TP:B11, *AVSN* = 32 dB) [redacted] (TP:G10, *AVSN* = 7 dB). *AVSN* is calculated per equation (8).

S vs. N plots are instructive and a useful tool for measurement debugging. However, for sifting through large data bases a single figure of merit quantifying the S/N properties is required. Therefore, the following figure of merit was developed for S/N quantification:

$$AVSN = \frac{1}{N}\sum_{n=1}^{N} f(n) \qquad (dB) \tag{8}$$

where

$$\begin{aligned} f(n) &= S/N \quad \text{if} \quad S/N > 6dB \\ &= 0 \quad \text{if} \quad S/N \leq 6dB \end{aligned} \tag{9}$$

[redacted]

Quality of Fourier Transforms: If the signal to noise ratio is low for a measurement, the true (but not measurable) signal lies below the measured noise. Thus, the measurement constitutes an upper bound on the true signal at the test point. Noisy measurements can still be extrapolated and Fourier transformed, but the resulting transient may not be accurate. A measure of this inaccuracy is obtained by performing sine (or odd) and cosine (or even) transforms, and comparing the resulting transient. Ideally they would be equal. This is illustrated in Figure 15, which shows the even and odd transforms for two extrapolated currents measurements.

Again a figure of merit is needed to perform an automated sift through large data bases for Fourier tranform quality control. Such a figure of merit is a Fourier tranforms error (FTE) defined by:

$$FTE = \frac{1}{M}\sum_{m=1}^{M} \frac{| f_e(t_m) - f_0(t_m) |}{PKI} \tag{10}$$

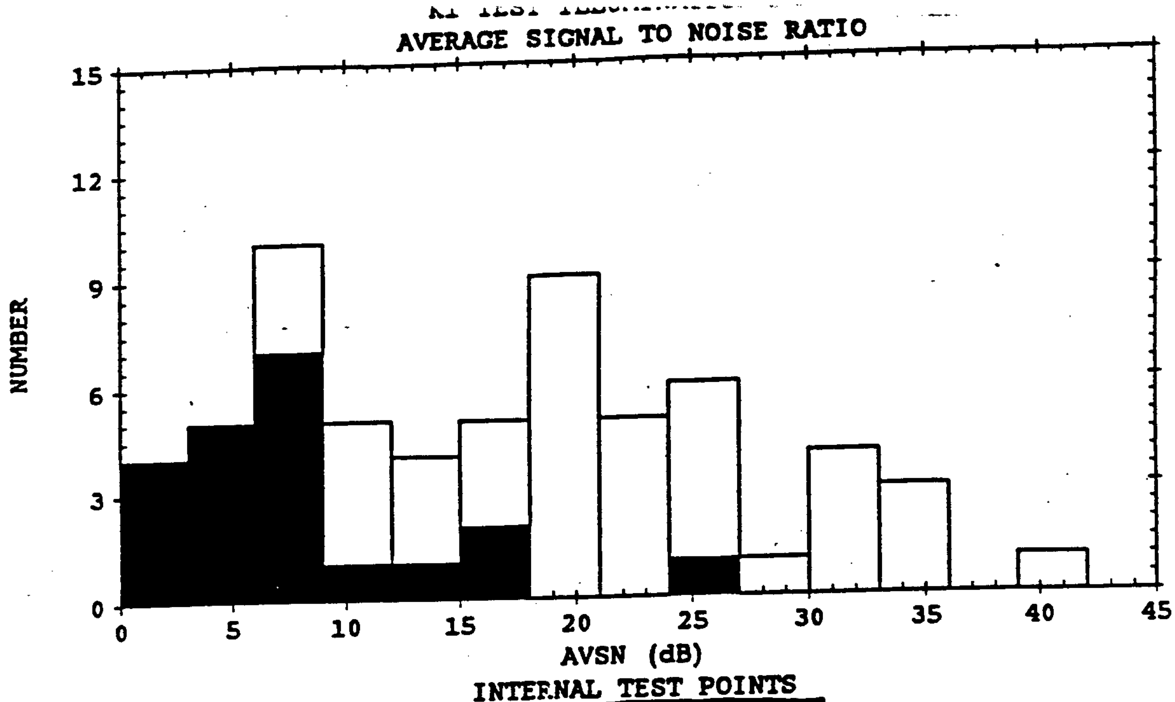

[redacted]

Figure 14. Average Signal to Noise ratios [redacted] for 62 measurements acquired in various areas [redacted]

FTE is a unitless quantity and measures the area between the even and odd transforms, normalized to the peak of the odd transform. Therefore, perfect transforms have FTE = 0. As a rule of thumb based on judgment, good transforms have FTE values less than 0.3.

One would expect a causal relationship between Signal-to-Noise ratios and quality of Fourier transform. Specifically, for poor *S/N* (small *AVSN*) the quality of the transform should also be poor (large FTE). The scatter plot of FTE vs. *AVSN* in Figure 16 confirms that the two figures of merit are correlated.

Upper Bound: Upper bounds exist for several waveform norms, which can be used to bound poor Fourier transforms. For example, the peak is bounded by the norm PINT:

$$PKI = \max_t \mid f_0(t) \mid = \frac{1}{\pi} \mid \int_{f_0}^{f_1} F(\omega) e^{j\omega t} d\omega \mid \leq \frac{1}{\pi} \int_{f_0}^{f_1} \mid F(\omega) \mid d\omega = PINT \quad (A) \quad (11)$$

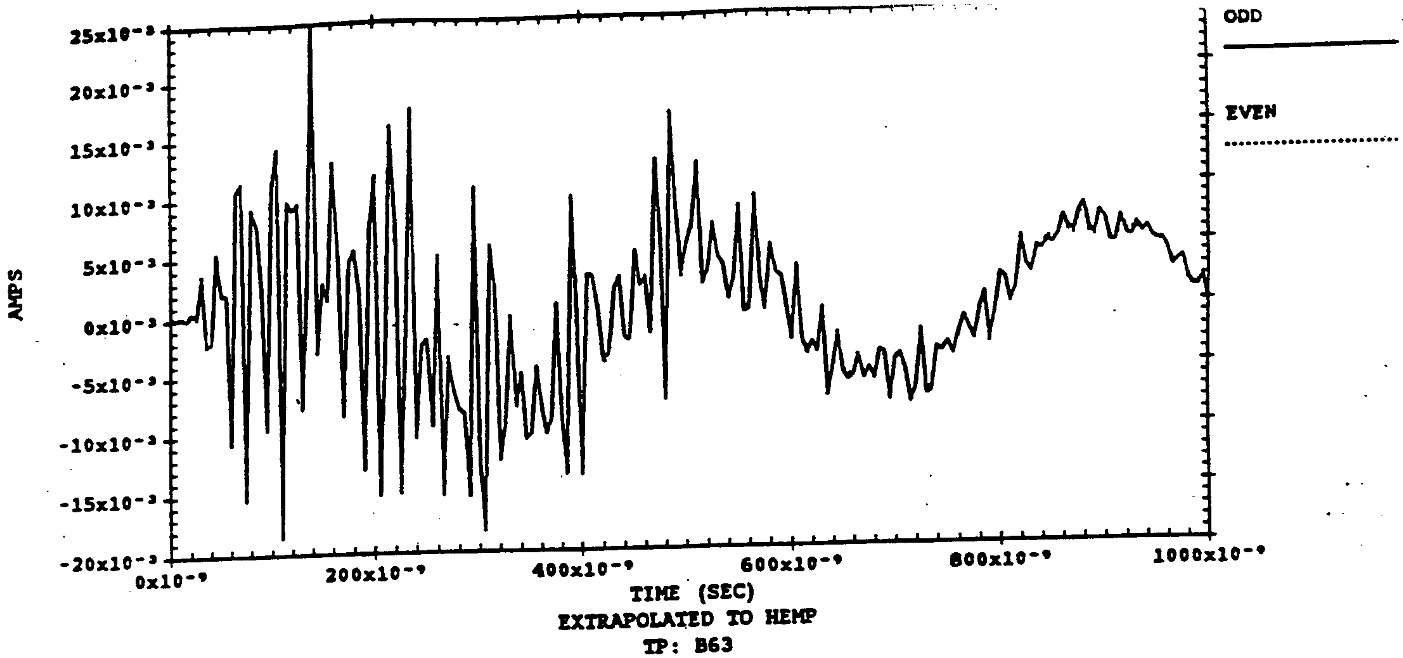

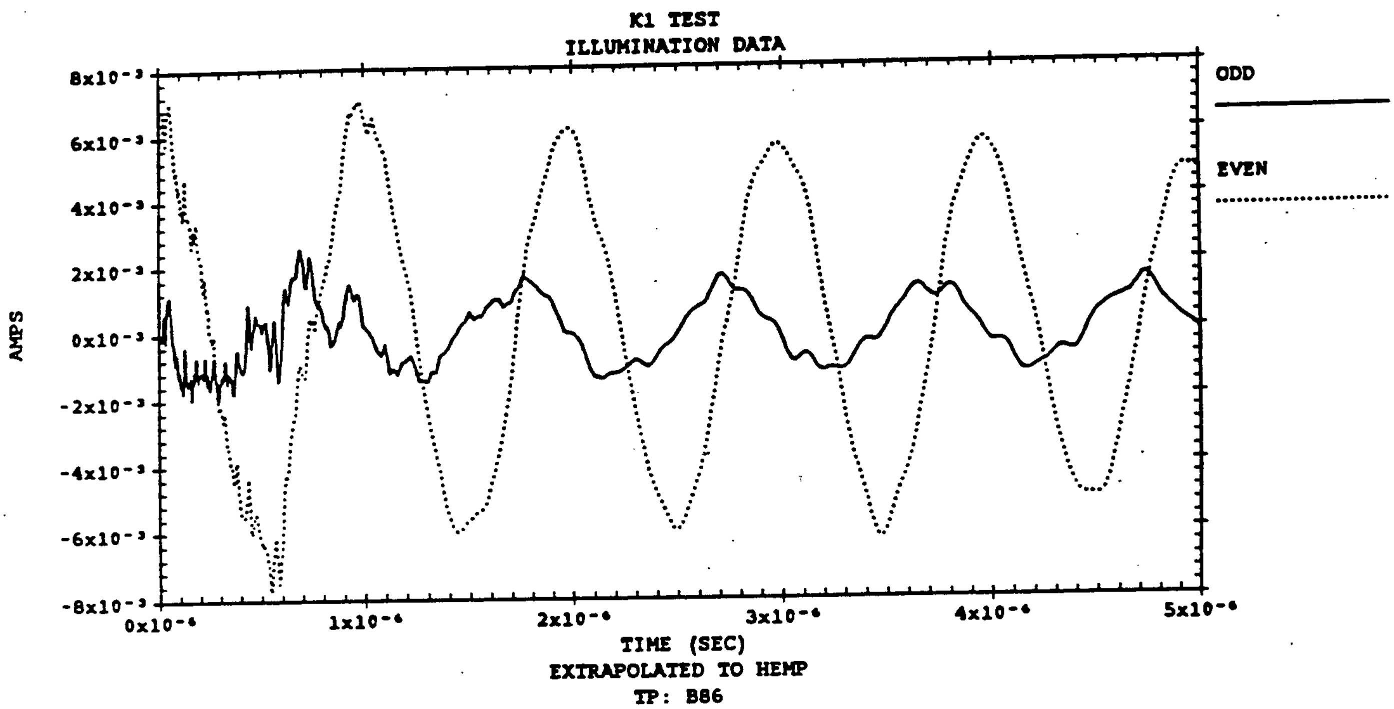

Figure 15. Even and odd tranform examples for a good transform (TP: B63, FTE = 0.05), and the poorest tranform (TP: B86, FTE = 1.54). (FTE calculated per equation (10)).

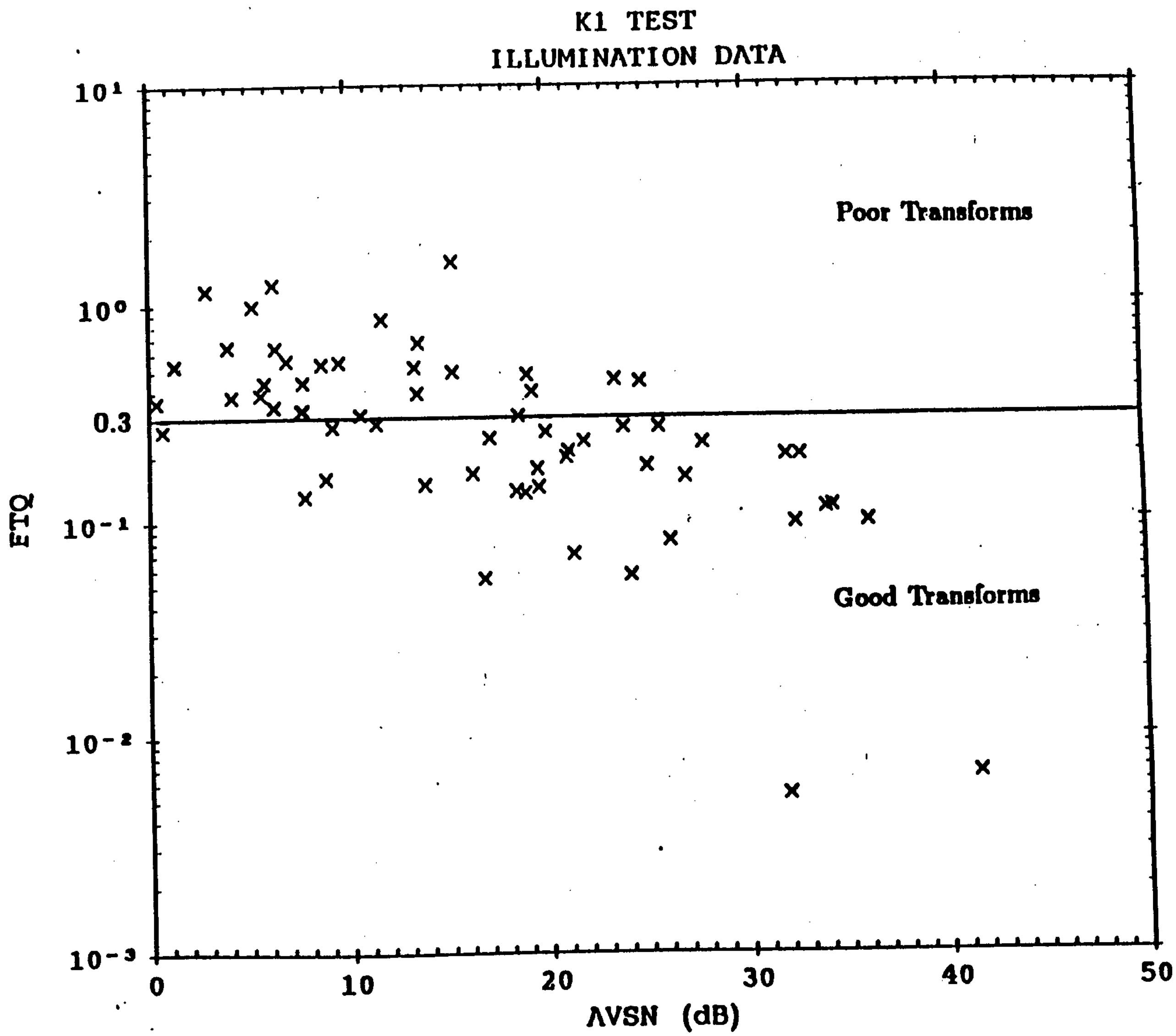

Figure 16. Scatter plot of tranform quality [redacted] vs. S/N ratio [redacted].

where f_0 and f_1 are 100 kHz and 100 MHz, respectively. Thus, PINT is a sure safe upper bound, and it is conservative by about a factor of 2 (6 dB). Upper bounds are further discussed in Appendix A.

The HEMP stresses [redacted] are quantified in terms of PKI (the peak of the odd transform) and PINT in the next sections.

2.3.1.2 CABLE CURRENTS [redacted] The illumination test measurements were extrapolated as described in Section 2.1, and Fourier transformed. The results are shown in Figure 17 in terms of peak currents (PKI) for good transforms, and in terms of the upper bound PINT for poor tranforms (FTE > 0.3). [redacted]

Except for test point B62, all peak currents and peak upper bounds PINT lie below 50 mA, and most are less than 20 mA. [redacted]

It also must be remembered that with low level CW illumination only the linear protection devices are evaluated. Hence, the presented HEMP current estimates may be somewhat higher than the actual HEMP currents. However, since the only nonlinear hardening devices are MOVs on the [redacted] the estimates based on CW are probably not overly conservative. This is further investigated with high level direct drive test data in Reference 8.

2.3.1.3 ERROR BOUNDS The previous section contains the estimates for HEMP induced currents inside [redacted] These estimates were obtained by scaling the CW illumination test measurements to a HEMP environment.

Since the illumination test cannot perfectly replicate the actual HEMP field spacial distribution [redacted] these estimates are not exact. Specific deficiencies are:

1. The field exciting [redacted] was not a uniform plane wave.

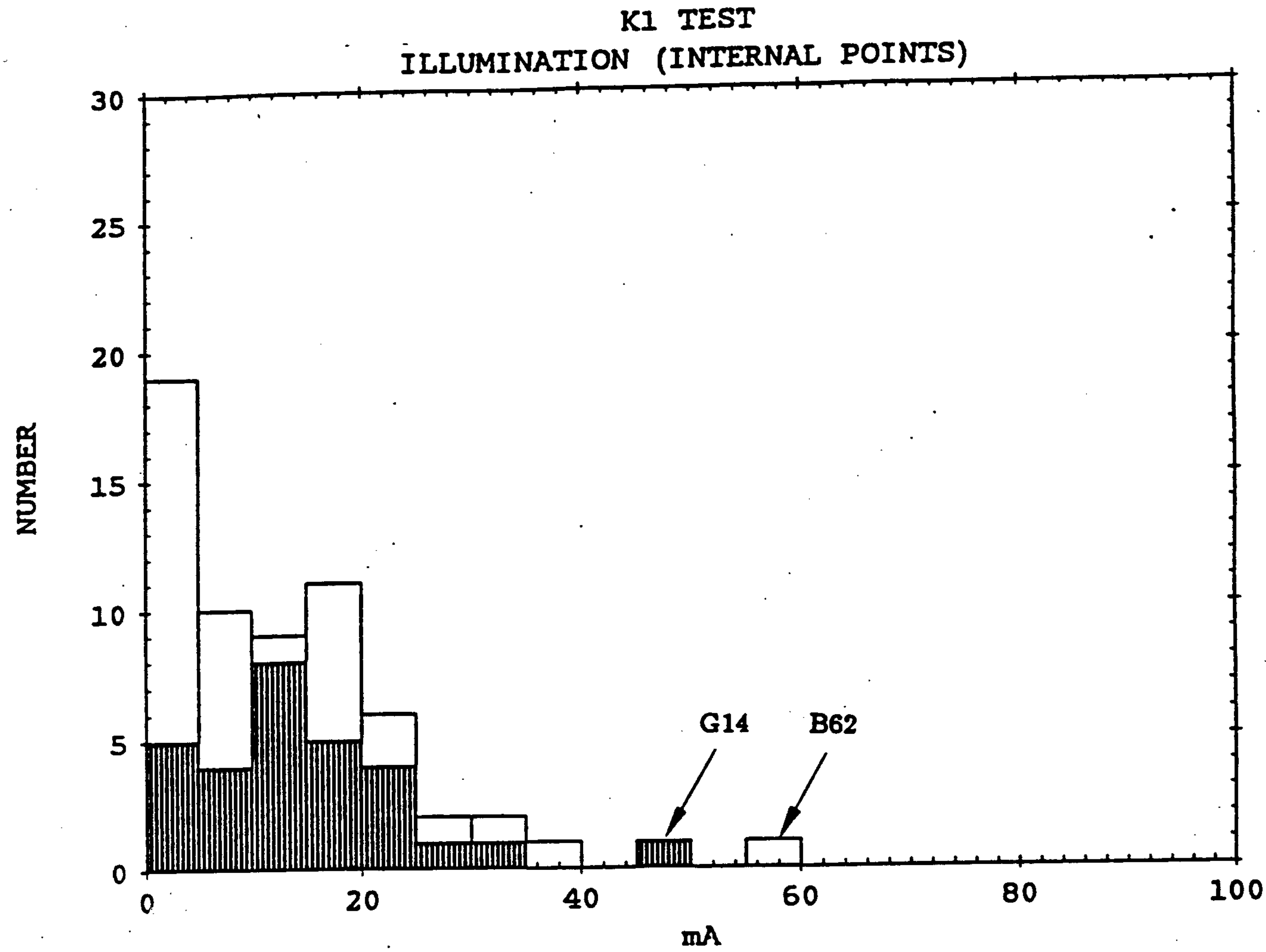

UNSHADED - PKI (FTE < .3)
SHADED - PINT (FTE > .3)

Figure 17. Peak HEMP current estimates [redacted] PKI shown for 33 test points (good transforms), and upper bound PINT (shaded) at 29 test points.

2. [redacted] was not illuminated with a plane wave.

3. The simulation antenna was only located in one position, namely to the south [redacted] oriented east-west. Therefore the building and the penetrations on the north side were on the shadow side, i.e., not strongly illuminated.

4. The measurement quality is not perfect at all internal test points due to the presence of ambient noise.

These error sources are discussed in the following.

1. [redacted] It was shown in Sections 2.2.2.1 and 2.2.2.2 that the extrapolated external [redacted] currents are 13 to 16 dB too low. Consequently, the HEMP current estimates may be low at internal test points which are connected [redacted]. Since the correction factor CORR(f) defined in Section 2.2.1 is not constant with frequency but varies considerably, a more accurate estimate of the error is obtained by applying CORR(f) to internal measurements.

Table 2 lists the peak HEMP current estimates (from Section 2.3.1.2) [redacted] The spectra of these 11 currents were then multiplied by CORR(f), and the product inverse transformed. The column entitled "Scaled by CORR(f)" contains the resulting peaks. The last column shows the ratios expressed in dB. Thus the average error is 11.7 dB or a factor of 4. Therefore the error of the HEMP stress estimates at East SAMT test points is approximately 12 dB. This bound is conservative because CORR(f) overestimates the effect of the illumination deficiency (cf. Section 2.2.1). This is the only applicable error because the three SAMTs are electrically well isolated as shown [redacted] bulk direct drive measurements. [redacted]

Since the inverted-V antenna used in the illumination test has been shown to be symmetric with respect to the centerline (x-axis), the 12 dB error bound also approximately applies [redacted]

[redacted] situation becomes more complicated because these test points are connected (in the sense that there is a signal path, not necessarily hardwire) [redacted]. It would certainly be conservative to apply a 24 dB error bound to all stress estimates in these two rooms. However, it would probably also be quite unrealistic because the stresses at these locations [redacted]. In [redacted]

Table 2. [redacted]

[redacted]

weak at HEMP frequencies, [redacted]

2. [redacted] was clearly not illuminated with a plane wave, but the currents induced are not small. [redacted]. To calculate a numerical error bound it would be necessary to compare the CW illumination measurements with more accurate and reliable data. However, for the particular HEMP illumination simulated [redacted] it is expected that this error bound would be small, and perhaps even negative, indicating that the CW illumination results are actually overestimates.

[redacted].

3. The CW illumination did not adequately test the integrity of the north building wall because only a single antenna position was possible within the time constraints of the test. (Data on the shielding effectiveness of the north wall were

acquired in MIL-STD-285 tests performed under the HDL test effort.) [redacted] Section 3.2 shows that the telephone penetration protection works well, and moreover the telephone cable [redacted] (The commercial power was pulse direct driven [redacted] Therefore, the stress contributions through the [redacted] re probably small, but in any event cannot be quantified with the CW test results alone except for the telephone penetration.

4. Ambient Noise: As discussed in Section 2.3.1.1, the facility generated noise interfered with the CW test signal. However, since the measurements are signal plus noise, the stress estimates are automatically conservative, and no additional error bound is needed.

For measurements yielding poor Fourier transforms, the norm PINT is used to bound the peak current. Again, PINT is already an upper bound, and thus no additional error bound is required.

In summary, 12 dB (factor of 4) is a conservative error bound for the HEMP stress estimates in Section 2.3.1.2, except perhaps [redacted] where the error cannot be defined. Thus, the histogram in Figure 17 would be shifted by a factor of four to bound the errors.

2.3.2 INTERNAL FIELD MEASUREMENTS

During the CWMS illumination internal fields were measured at two locations (D1, D2) [redacted] All measurements were taken 1 m above the floor.

A measure of the global shielding effectiveness is obtained by comparing the internal fields with the external fields. The dominant components of the incident field are E_y, H_x, and H_z. The fields inside the building are produced by diffraction, scattering, and reradiation from cable currents, hence there are no a priori preferred or theoretically dominant field components. Therefore, for completeness one would have to measure all six field components. However, such an exhaustive investigation into the merits of internal field mapping was not possible within the test schedule.

Page 34 deleted in its entirety.

There are important open technology questions associated with internal field mapping, such as:

- Is the CWMS capable of verifying compliance with a 100 dB shielding requirement? (Specifically, are its dynamic range and noise rejection features sufficient to measure fields 100 dB below the external simulation fields?)
- How many internal locations must be mapped, and where?
- How well are internal field map measurements correlated with MIL-STD- 285 measurements?

The internal field map [redacted] was performed only on an experimental basis to determine the usefulness of such measurements. Therefore, only the components identified in Table 3 were measured. Note that there are three configurations for [redacted] door *A9* (closed, open, and taped). Only measurements acquired in the normal configuration (door closed) are discussed in this section, the other two are deferred to the next section.

Data Quality: The ambient noise discussed in Section 2.3.1.1 also affects the quality of internal field measurements. Figures 19 and 20 show typical signal vs. noise comparisons for field measurements [redacted] Note that the [redacted] field measurement is completely dominated by noise, while [redacted] and especially at the [redacted] D2 location the CWMS test signal exceeds the noise by as much as 70 dB in the frequency range above [redacted]

Internal Fields due to HEMP: The internal field measurements were extrapolated as described in Section 2.1. The resulting bounds on the internal peak fields (PINT) [redacted] A complete list is contained in Table 4, Section 2.3.3.

Table 3. **Internal field components measured during CW illumination testing.**

Internal Field Map Location	[redacted] Configuration	Field Components Measured
[redacted] D1	[redacted]	E_x, E_z, H_x, H_z
D1		E_x, E_z
D1		E_x, E_z
D2	[redacted]	E_x, E_z, H_x, H_z
D2		E_z
[redacted] S1	[redacted]	E_x, E_z
[redacted] W1	n/a	E_x, E_z, H_x, H_z

Field Attenuation (FATT): A measure of shielding effectiveness or field attenuation is obtained by dividing the internal field measurements by the external field. It seems that the most unambiguous form of the external field is the incident field. Thus the attenuation of electric fields (EFATT) is defined by:

$$E_a FATT(f) = -20 \quad log \left| \frac{E_a^{int}}{E^{inc}} \right| \qquad (dB) \tag{12}$$

where E_a^{int} is one of the three internal electric field components. Similarly, the attenuation of magnetic fields (HFATT) is defined by:

$$H_a FATT(f) = -20 \quad log \left| \frac{H_a^{int}}{H^{inc}} \right| \qquad (dB) \tag{13}$$

where H_a^{int} is one of the three internal magnetic field components. Note that these definitions are independent of ground conductivity, angle of incidence (antenna standoff distance), and other test conditions.

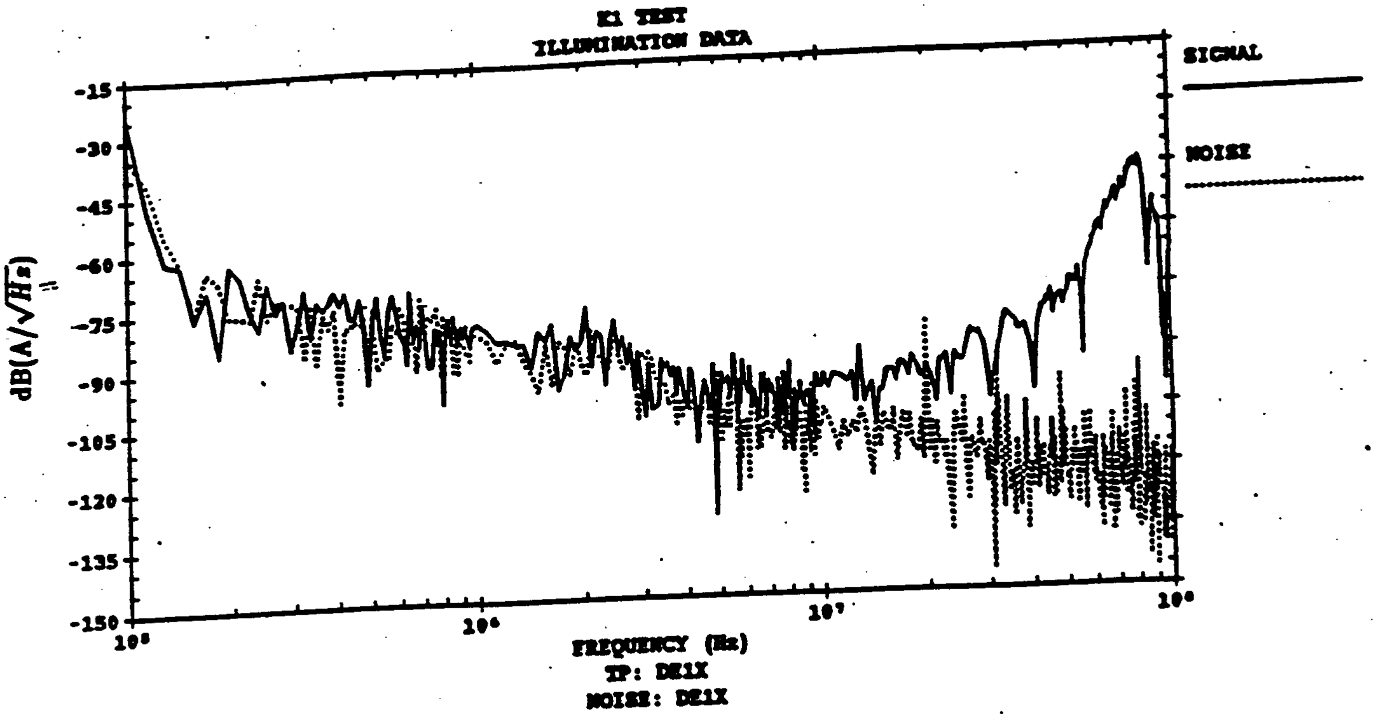

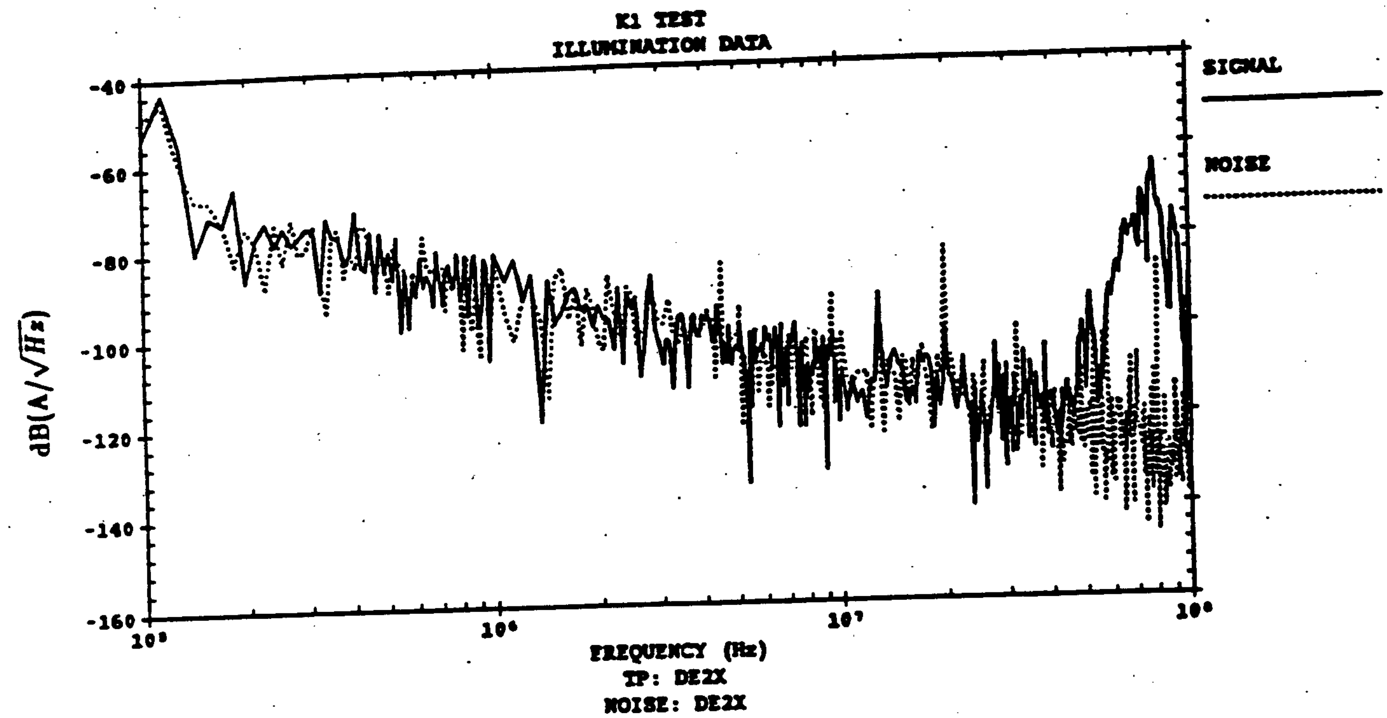

Figure 19. **Internal field map signal vs. noise examples** [redacted] **at** [redacted]

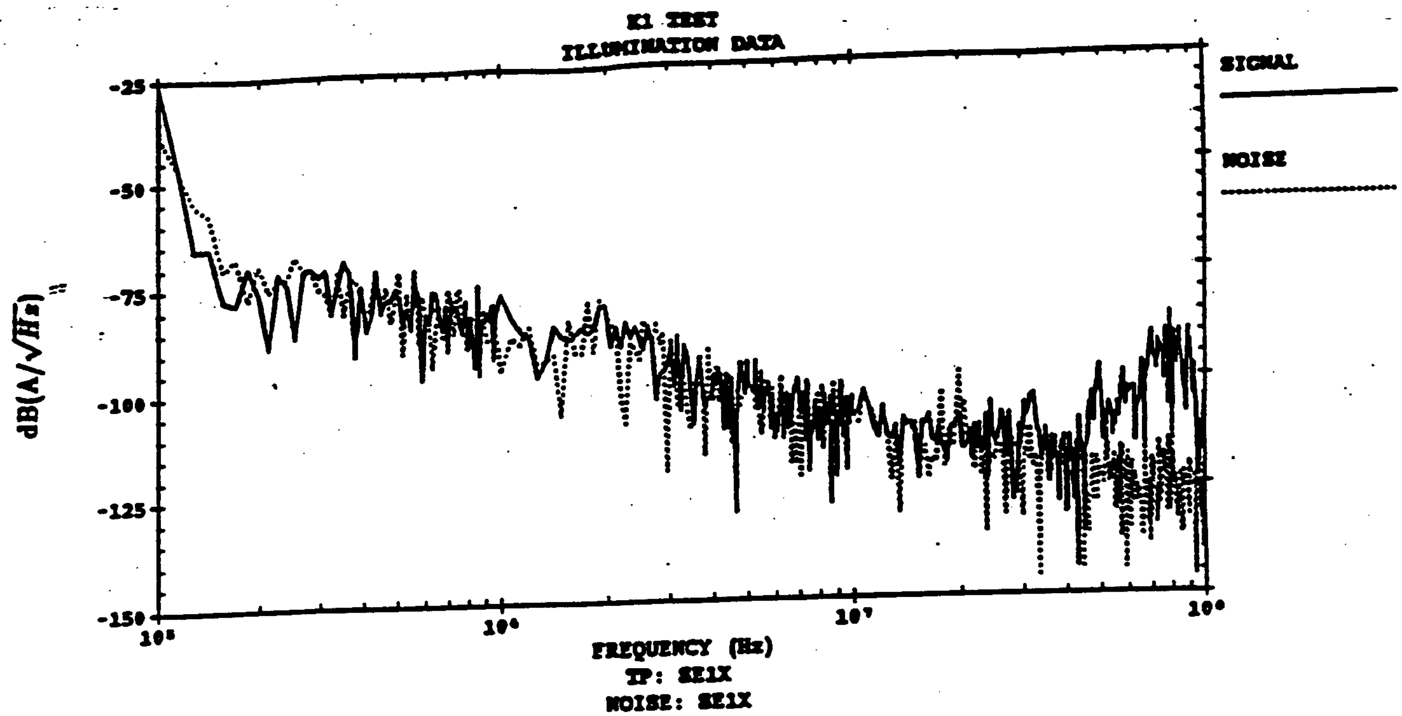

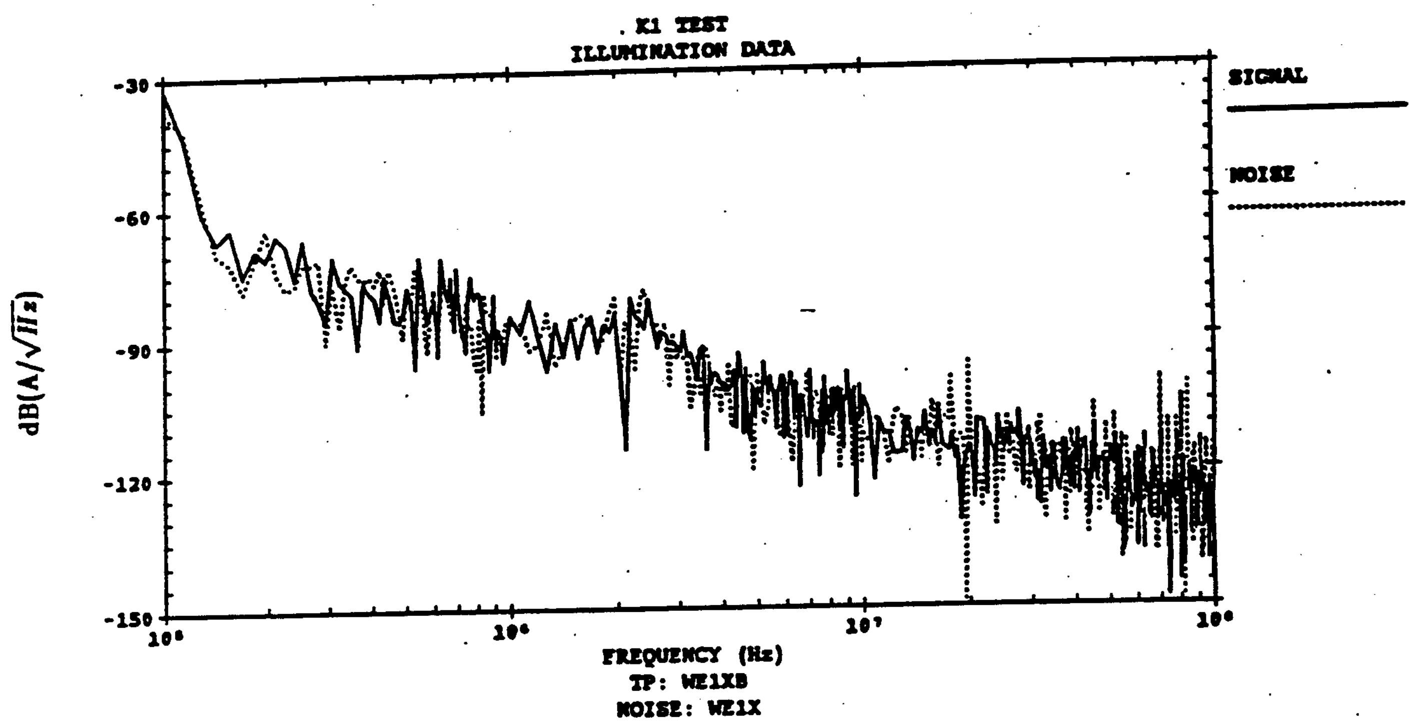

Figure 20. Internal field map signal vs. noise examples [redacted] and [redacted] rooms.

FATT is to divide the extrapolated measurements by the incident HEMP spectrum. For example, EFATT for the x-component is

$$E_xFATT(f) = -20 \ \log \left| \left(\frac{E_x^{int}}{H_x(R)} \right)_{ill} \frac{H_x^{thr}}{E^{inc}} \right| \quad (dB)$$

$$H_xFATT(f) = -20 \ \log \left| \left(\frac{H_x^{int}}{H_x(R)} \right)_{ill} \cdot \frac{376.7 H_x^{thr}}{E^{inc}} \right| \quad (dB) \qquad (14)$$

The FATT was calculated for all four locations [redacted] and the results are shown in Figures 21 to 24. For comparison, the FATT requirements of MIL-STD-188-125 (Draft) are included.

These figures show that the 100 dB electric field attenuation cannot be demonstrated [redacted] because the internal field measurements are noise dominated as seen from Figures 19 and 20. Moreover, at frequencies abov[redacted] electric field attenuation proposed in MIL-STD-188-125 [redacted]). However, [redacted] the 100 dB attenuation requirement was met [redacted].

On the other hand, the magnetic field attenuation required by MIL-STD-188-125 [redacted]

Thus, the CWMS data acquisition equipment possesses a sufficiently great dynamic range to demonstrate compliance with the proposed field attenuation curves [redacted] In a subsequent revision of MIL-STD-188-125 the electric field attenuation requirement was limited to the range 5 MHz to 100 MHz. [redacted] the CWMS was able to demonstrate 100 dB electric field attenuation over this modified range despite the noise.

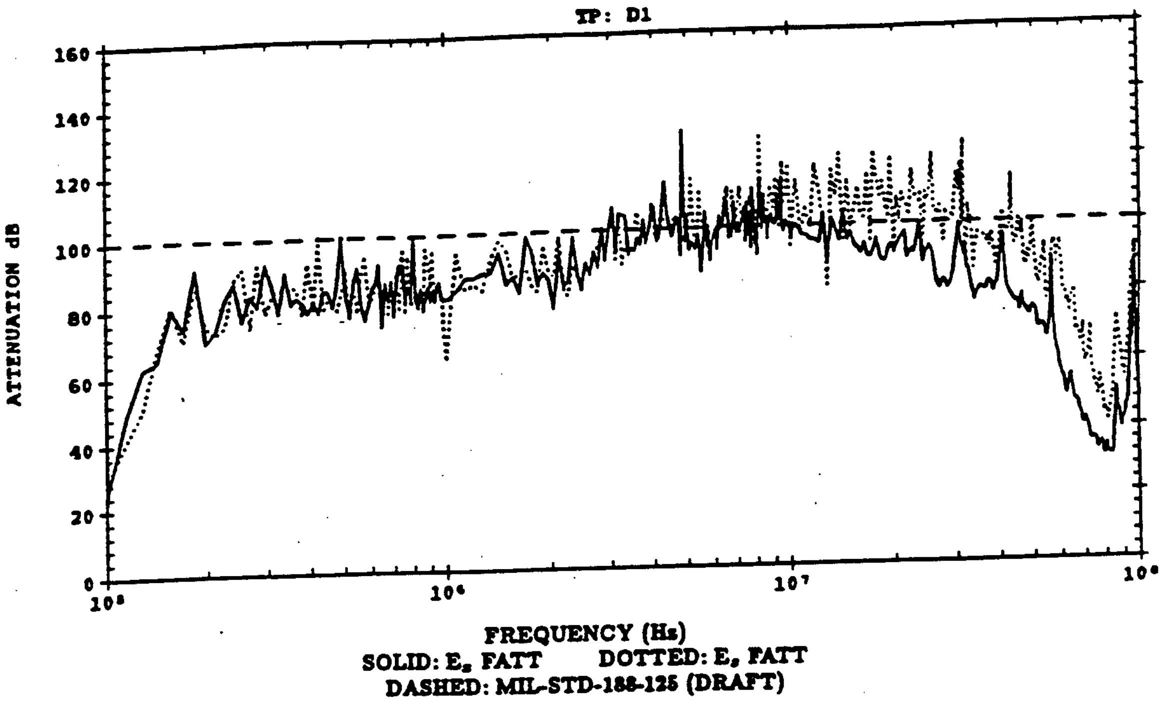

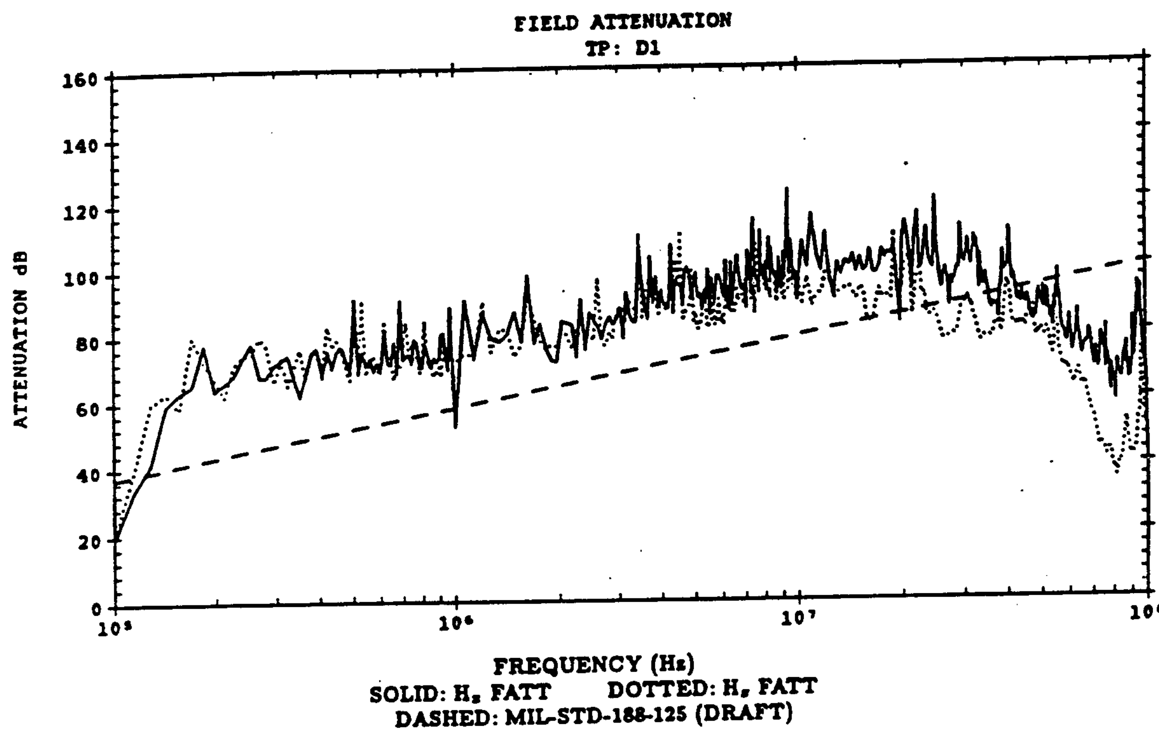

Figure 21. Electric (E_zFATT, E_yFATT) and magnetic field attenuation (H_zFATT, H_yFATT) [redacted] location D1, [redacted], vs. FATT required per MIL-STD-188-125 (Draft).

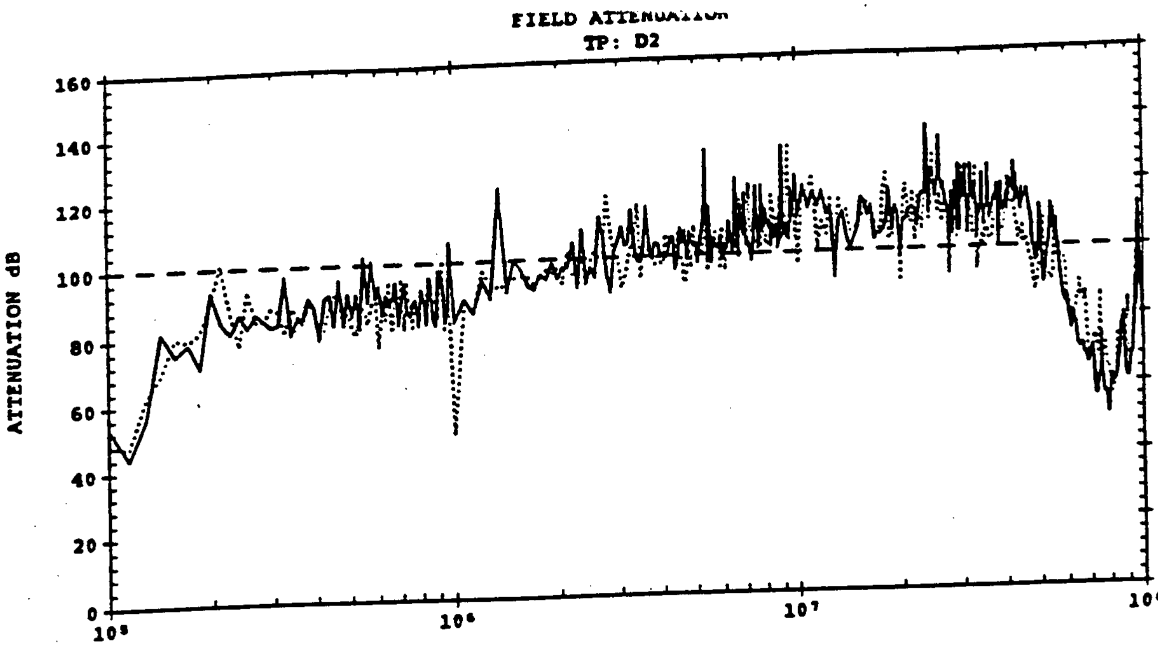

FREQUENCY (Hz)
SOLID: E_z FATT DOTTED: E_r FATT
DASHED: MIL-STD-188-125 (DRAFT)

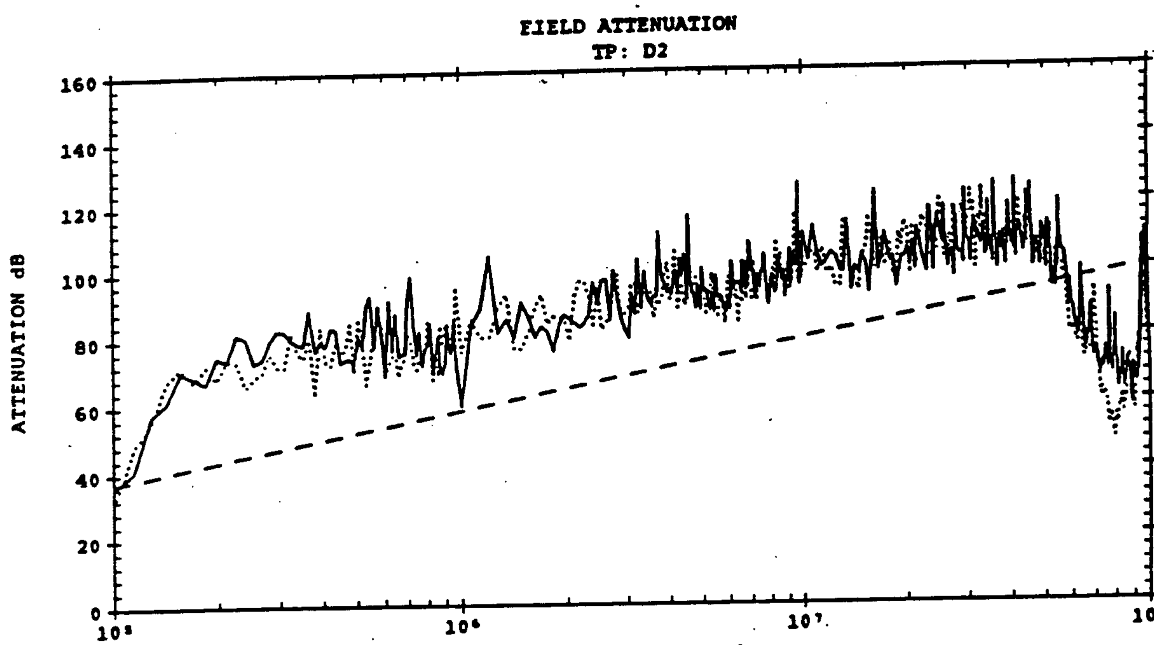

FREQUENCY (Hz)
SOLID: H_z FATT DOTTED: H_r FATT
DASHED: MIL-STD-188-125 (DRAFT)

Figure 22. Electric (E_zFATT, E_rFATT) and magnetic field attenuation [redacted]TT, H_rFATT) [redacted] (location D2, [redacted], vs. FATT required per MIL-STD-188-125 (Draft).

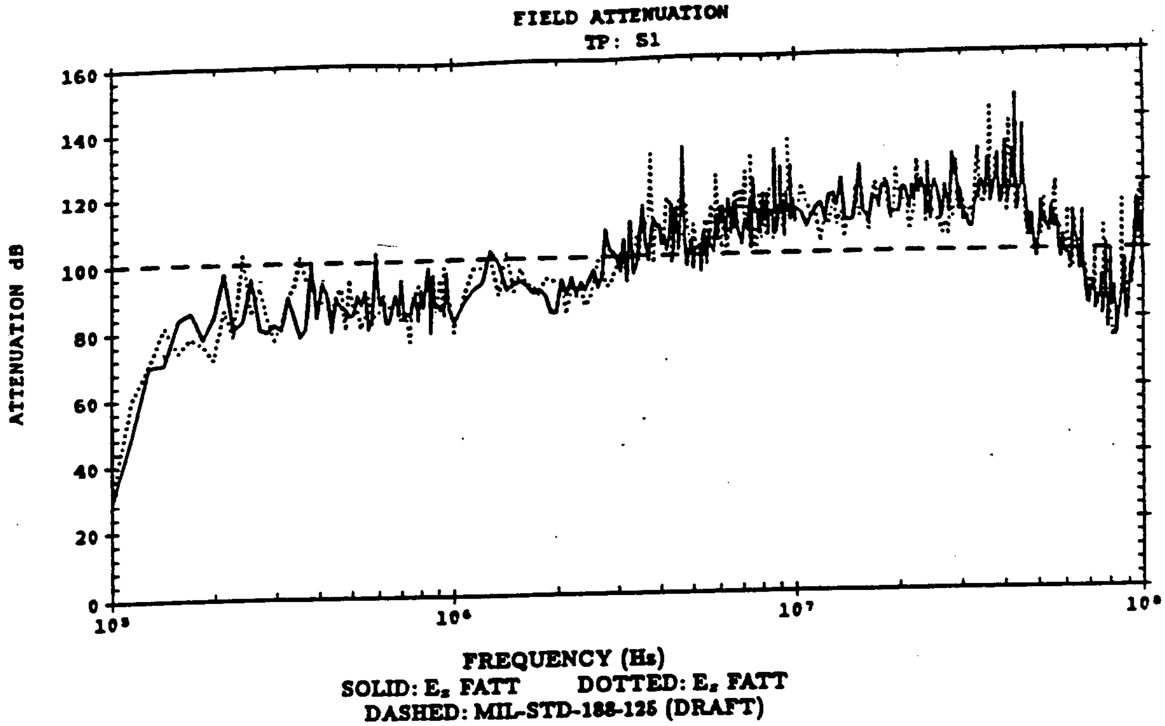

Figure 23. Electric field attenuation (E_zFATT, E_zFATT)[redacted](location S1, [redacted]), vs. FATT required per MIL- STD-188-125 (Draft).

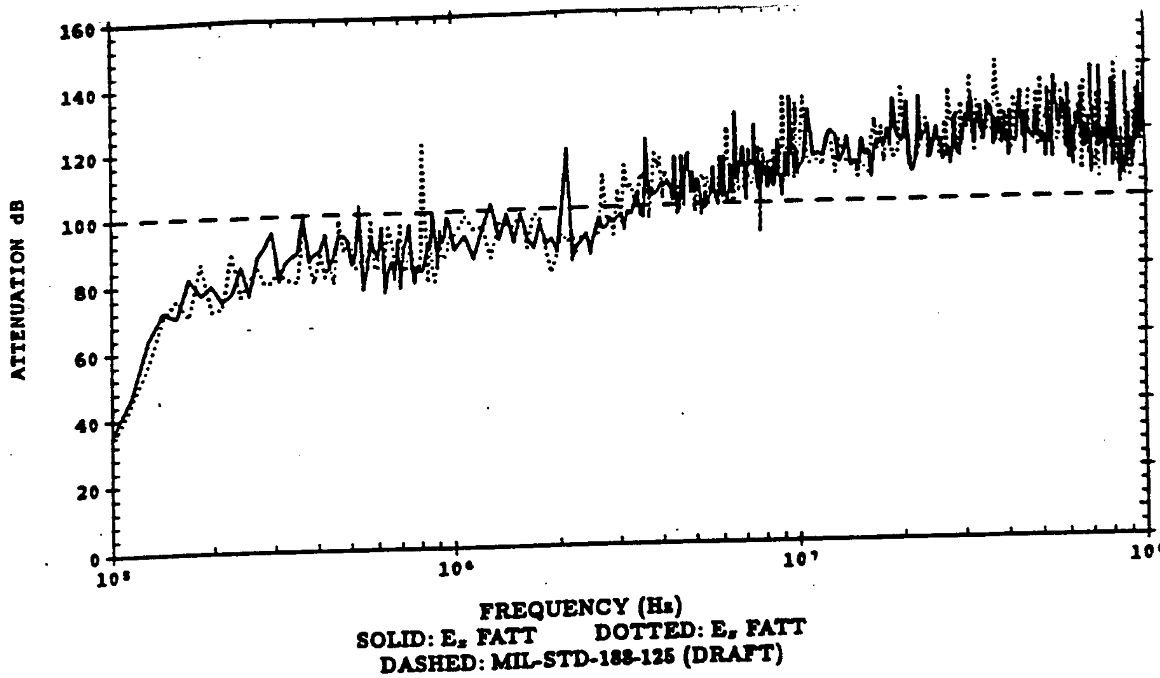

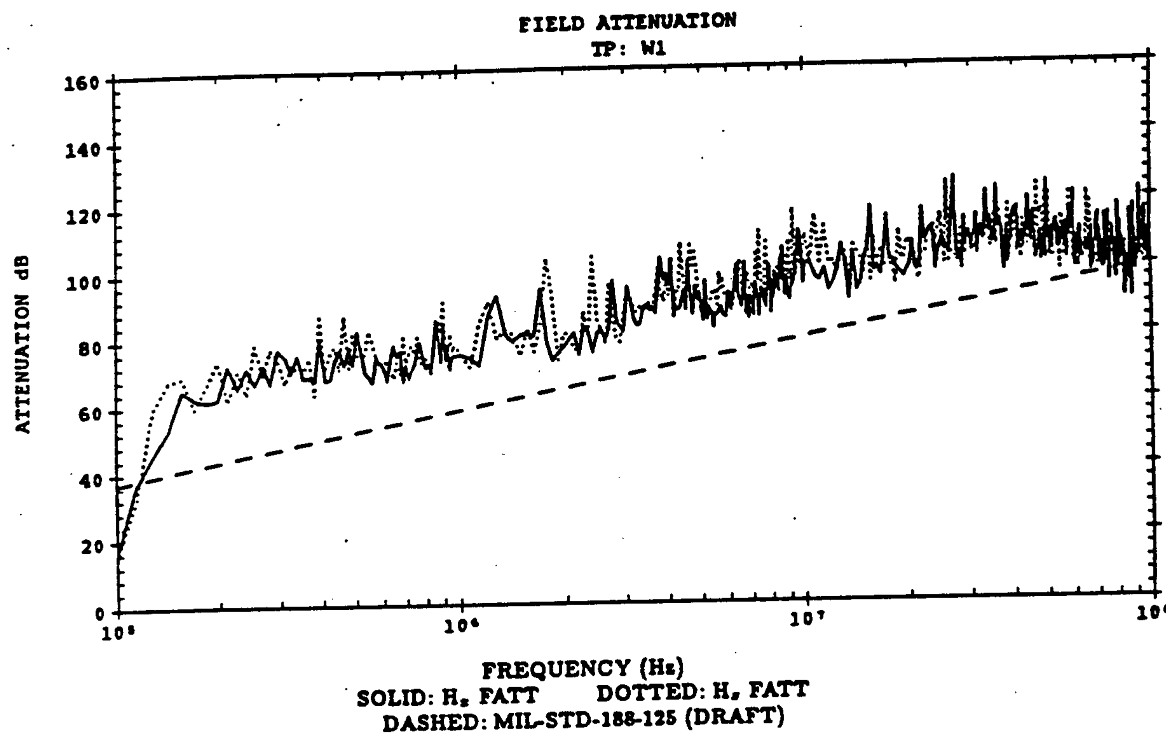

Figure 24. Electric (E_zFATT, E_yFATT) and magnetic field attenuation (H_zFATT, H_yFATT) [redacted] (location W1, [redacted]; vs. FATT required per MIL-STD-188-125 (Draft).

Page 44 deleted in its entirety.

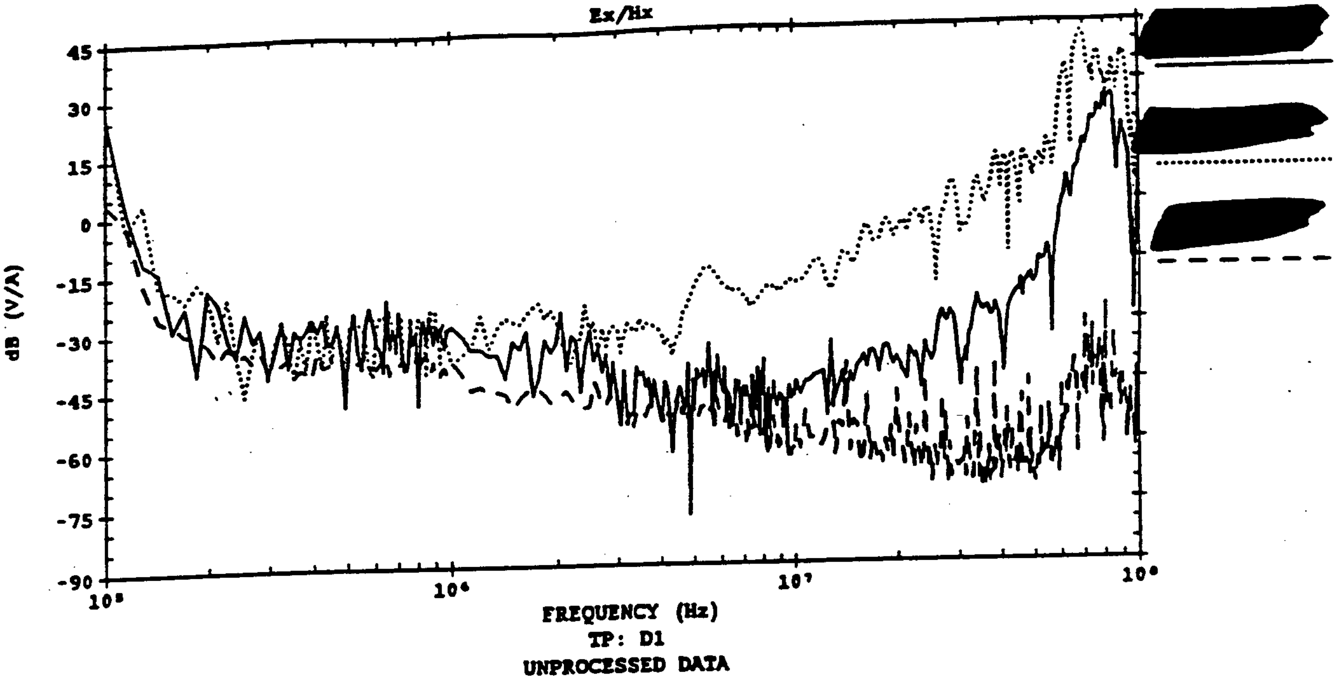

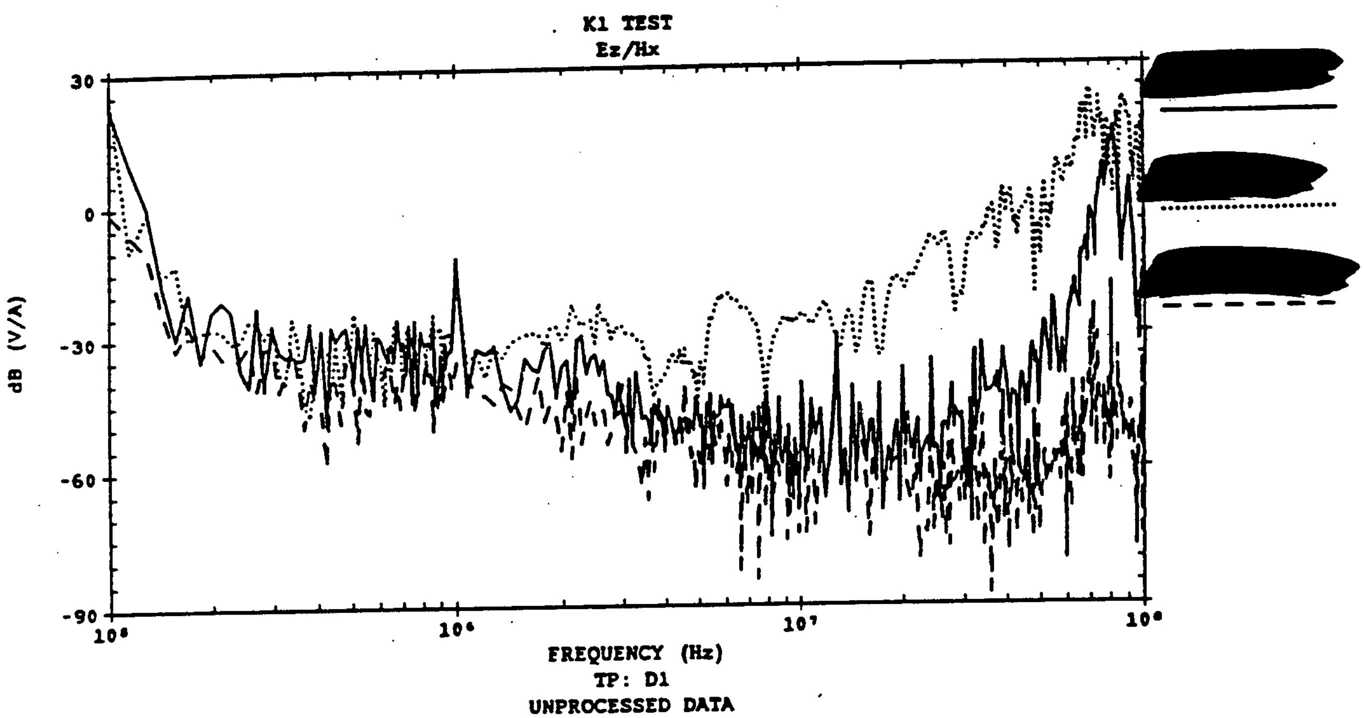

Figure 25. Internal fields E_x^{int} and E_z^{int} at test point D1; [redacted] (unextrapolated measurements).

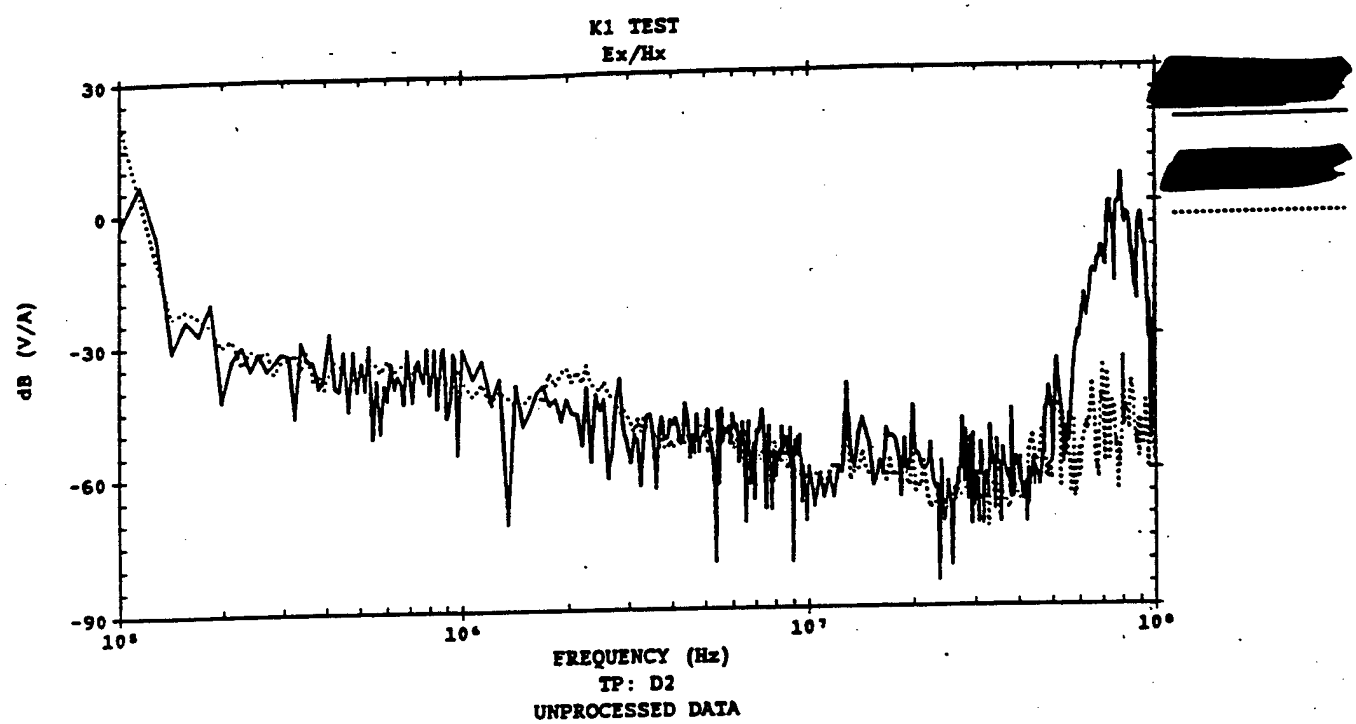

Figure 26. Internal fields E_z^{int} at test point D2; [redacted] (unextrapolated measurements).

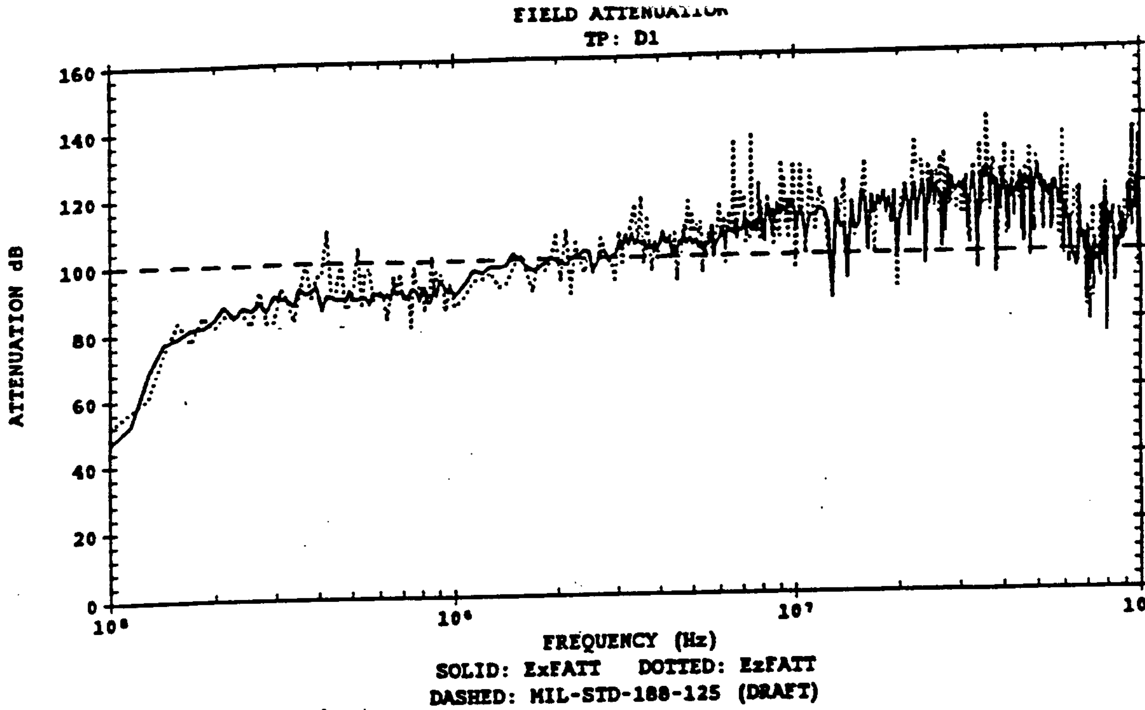

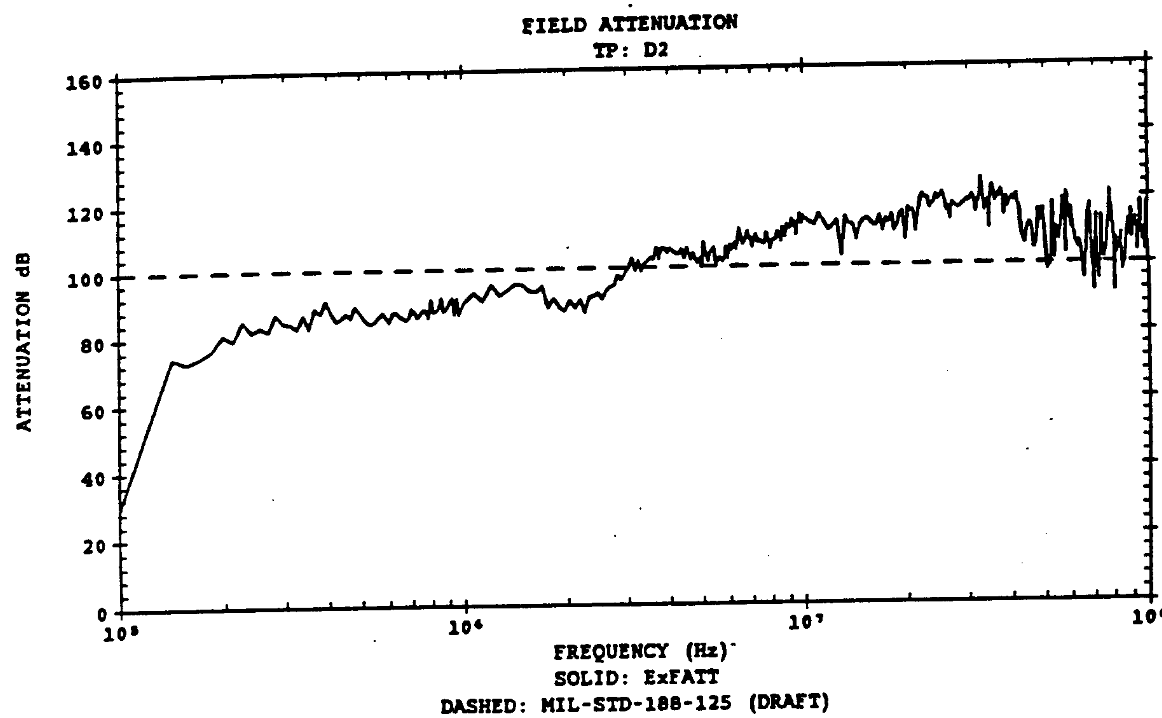

Figure 27. Electric field attenuation at locations D1 and D2 [redacted] [redacted] vs. FATT required per MIL-STD-188-125 (Draft).

Page 48 deleted in its entirety

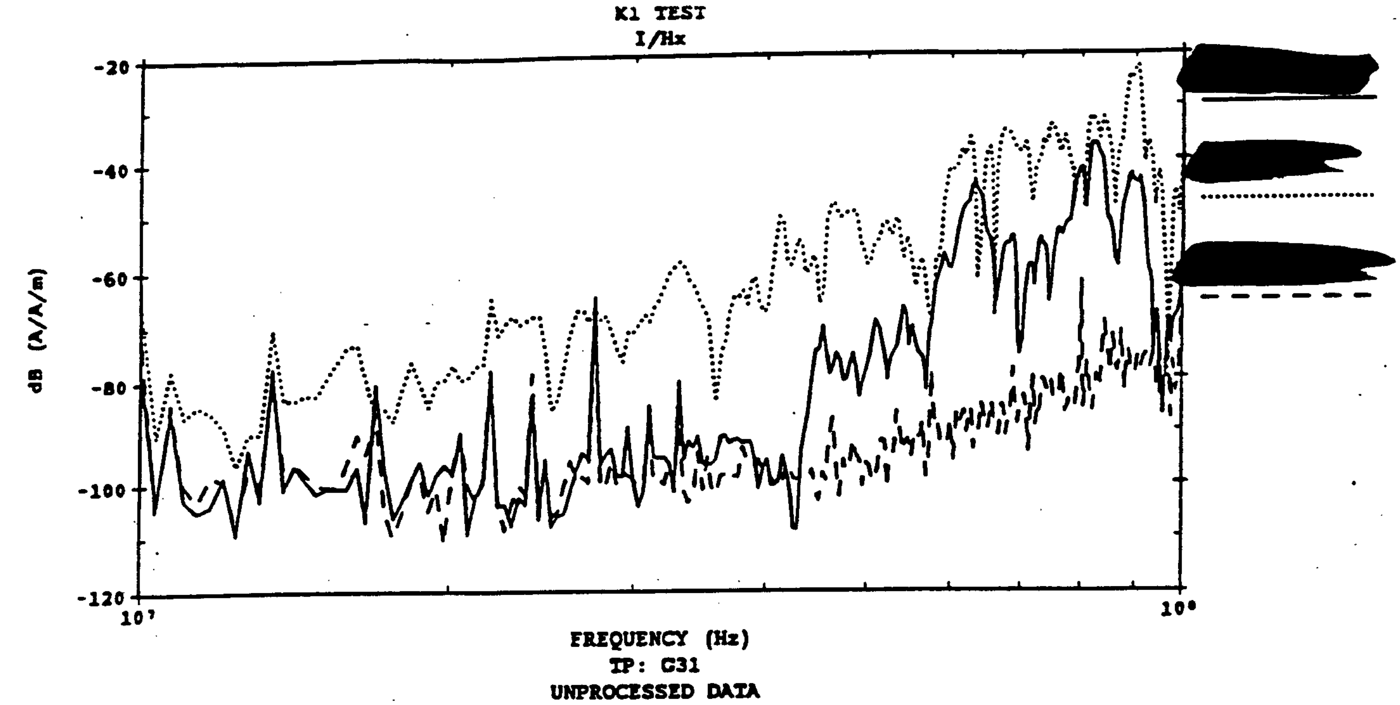

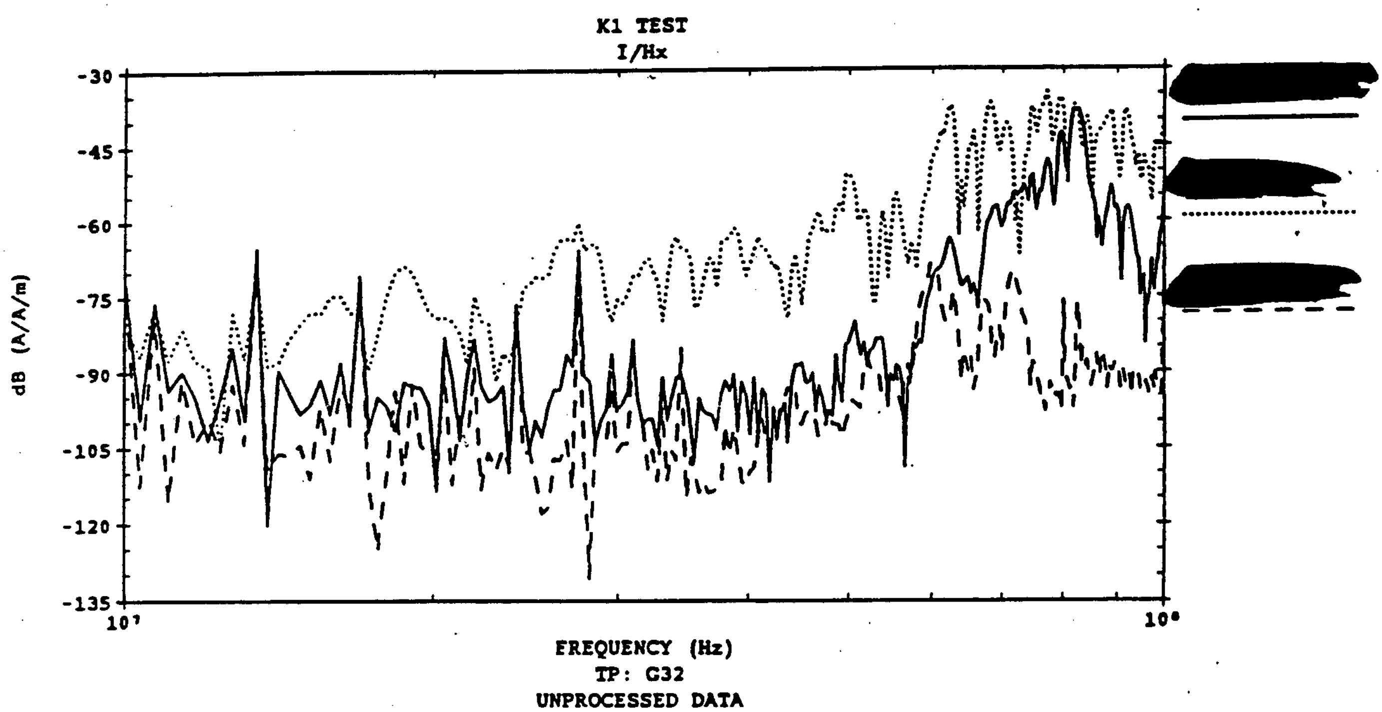

Figure 28. Unextrapolated measurements of cable currents at test points G31 and G32 for various [redacted] configurations. The measurements are plotted from 10 MHz to 100 MHz to enhance legibility. The narrow spikes are due to ambient noise.

Table 5. HEMP currents at test points G31 and G32 [redacted]

INTERNAL TEST POINT	[redacted]	PINT (mA)
G31	[redacted]	41.3
		186.7
		13.3
G32	[redacted]	29.7
		110.2
		9.9

.3.4 [redacted]

To compare the results from the two tests, the [redacted] measurements were extrapolated to the field defined in equation (15), and the upper bound on the peak current (PINT) as well as the root-action integral (RAINT) were calculated.

In Figures 29 and 30 the internal HEMP stresses [redacted] are compared in terms of PINT and RAINT. The results conform essentially with exceptions: [redacted]

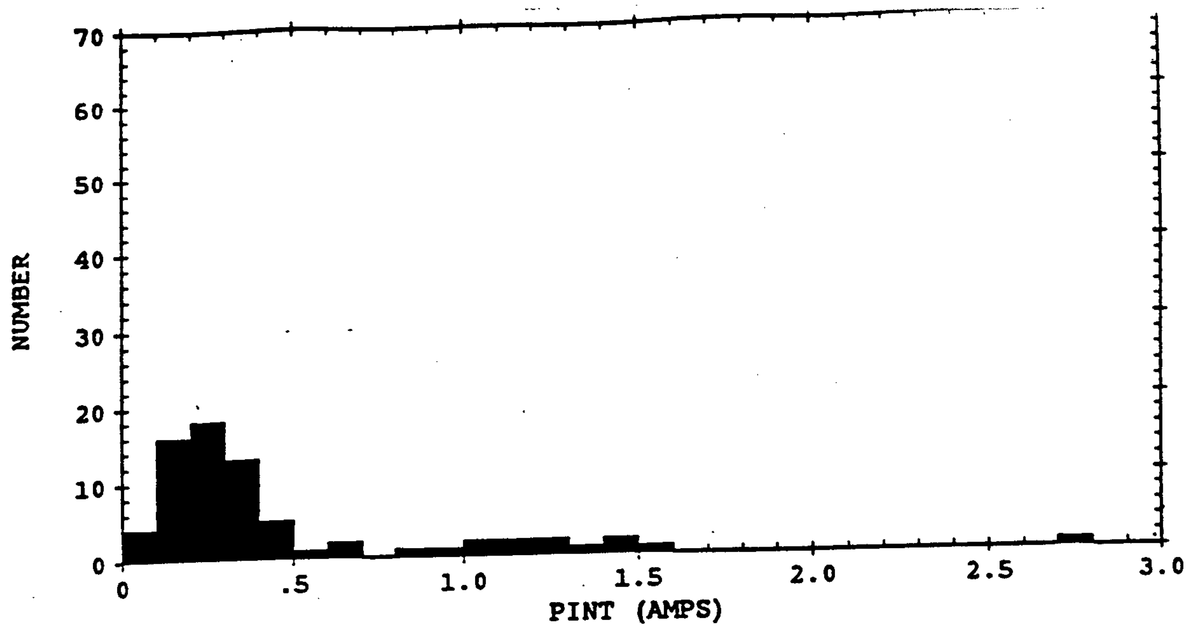

SURVEILLANCE TEST 2
ILLUMINATION DATA (INTERNAL)

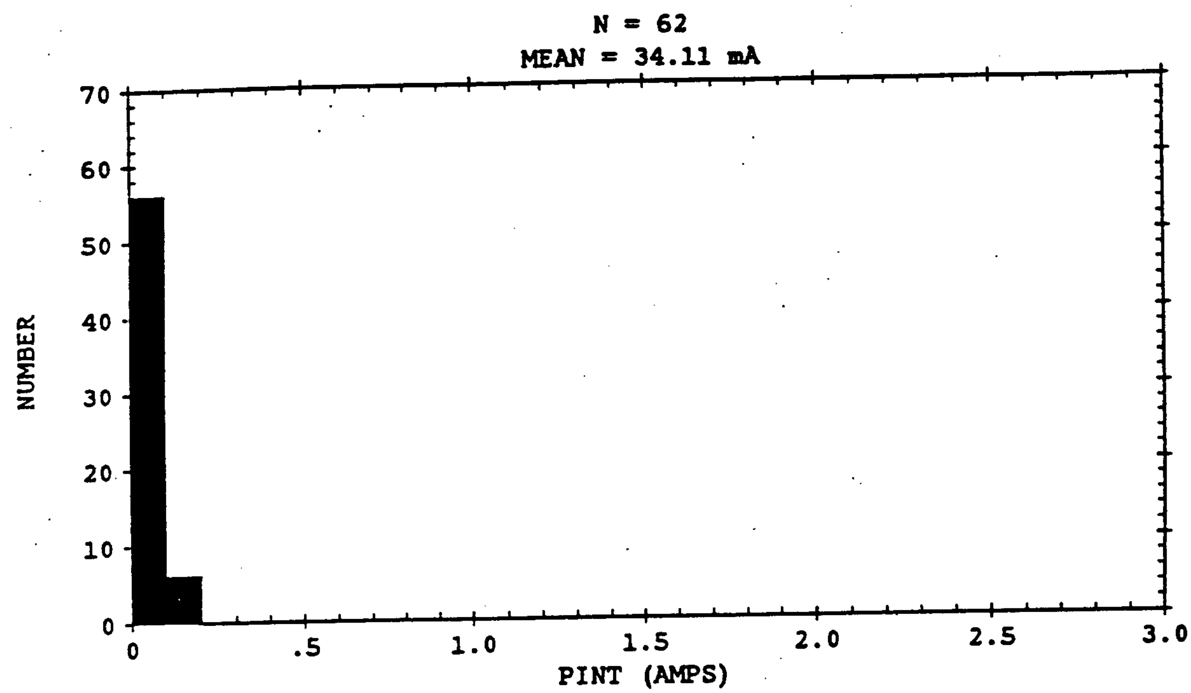

K1 TEST
ILLUMINATION DATA (INTERNAL)

Figure 29. Internal HEMP stresses [redacted] terms of PINT (both populations extrapolated to HEMP defined in equation (15).

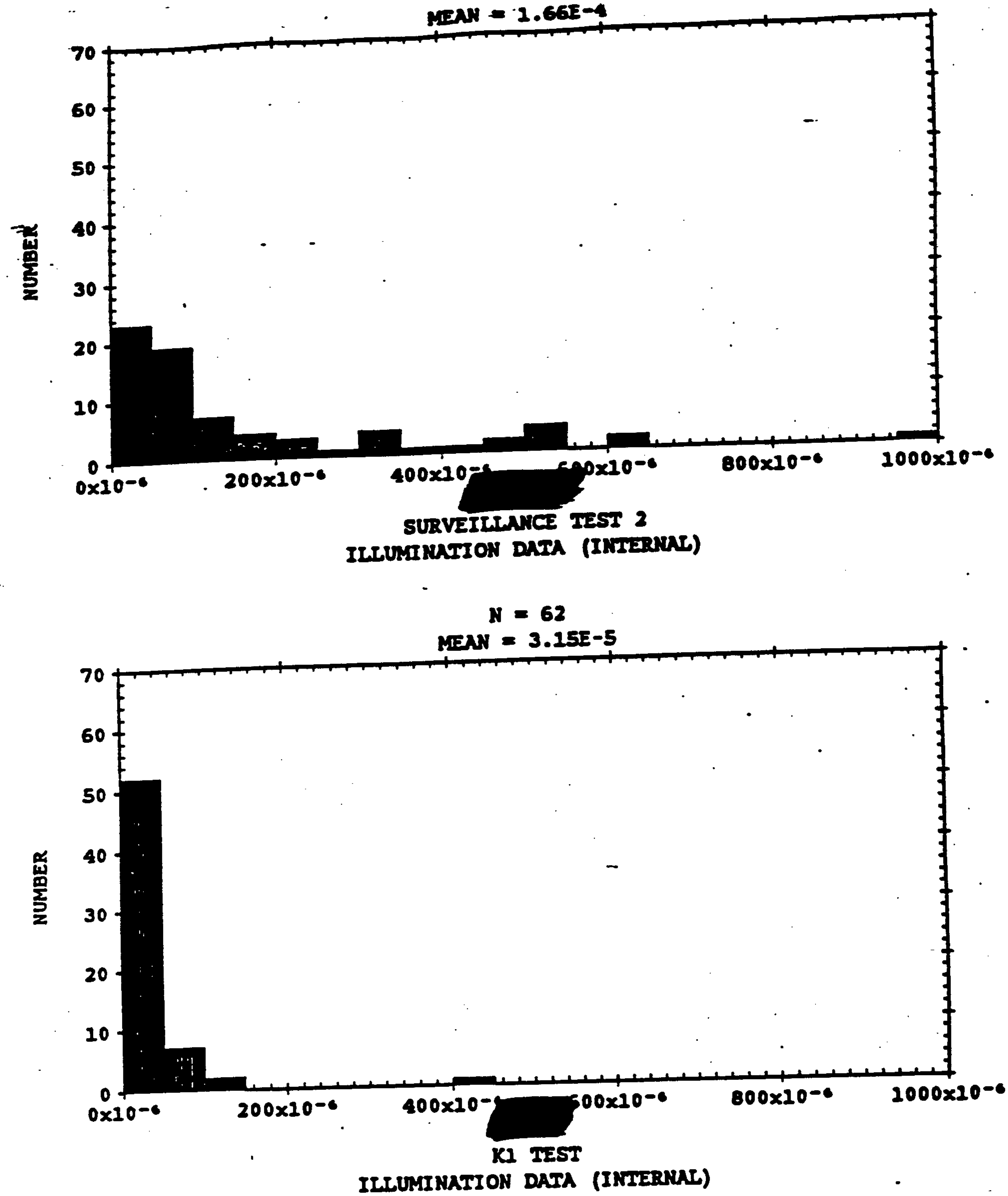

Figure 30. Internal HEMP stresses [redacted] terms of root-action integral [redacted] (both populations extrapolated to HEMP per equation (15).

SECTION 3

PENETRATION DIRECT DRIVE

[redacted] the telephone cable were externally direct driven, and measurements were acquired inside [redacted]. CW currents from 10 kHz to 100 MHz were inductively driven on these penetrations, and at internal test points the resultant currents were measured relative to the external excitation current.

Penetration direct drive tests serve the following purposes: To measure the insertion loss [redacted] and to determine the penetration or land line drive at internal test points.

Insertion Loss: It is a quantitative measure of the effectiveness of the penetration protection. The insertion loss can be compared to hardening specifications to demonstrate compliance. In addition, penetration protection faults can be detected with direct drive tests. However, CW direct drive tests only evaluate the linear protection features.

Land Line Drive: The HEMP stresses at internal test points are due to local coupling and land line drives (References 9, 10). Local coupling is caused by fields diffracting through apertures in the shield [redacted]. On the other hand, land line drives are caused by HEMP currents on external lines [redacted] The distinction between local coupling and land line drives is especially important for HEMP hardness verification testing: If land line drives dominate local coupling at internal test points, then high level pulse direct drive of the land lines provides a HEMP hardness verification because it stresses the dominant coupling mechanism. Thus, the CW direct drive tests performed support the rationale for the HDL high level pulse tests (Reference 2).

CW direct drive tests were performed [redacted] the telephone line penetration.

3.1 DIRECT DRIVE OF THE [redacted]

[redacted] externally direct driven at their entry point into the [redacted] nd measurements were acquired on cables [redacted]. Since the bulk direct drive technique is still in the experimental stage, only the single line direct drive results are discussed here; the bulk direct drive data are evaluated in a subsequent report (Reference 3).

Single line direct drive measurements are complex transfer functions of the form:

$$T(f) = \left(\frac{TP}{Ai}\right)_{SDD} \qquad (A/A) \tag{16}$$

where the numerator (signal) is the current measured at the internal test point (TP), and the denominator is the current driven on the shield of the external cable Ai. The subscript "SDD" indicates that the measurement is a single line direct drive. Since the transfer function was obtained using low level CW, equation (16) only predicts the linear transfer, i.e., it does not account for nonlinear protection features.

3.1.1 INSERTION LOSS

The measured transfer functions are the attenuation provided by the penetration hardening as a function of frequency[redacted]Figure 31 shows two typical examples.

Note that the attenuation varies considerably with frequency. Therefore, the attenuation cannot be readily and completely described with a single numerical value. To comprehend and compare the[redacted]measurements it is necessary to condense the data, i.e., another figure of merit is needed.

Since there does not appear to be a standard method of achieving this, after considering the options, the following figure of merit for insertion loss is defined:

$$IL(TP/Ai) = -20 \quad log \frac{1}{f_1 - f_0} \int_{f_0}^{f_1} |\, T(f) \,|\, df \quad (dB) \tag{17}$$

which indicates the external driven cable (Ai) and the internal test point (TP); and where f_0 and f_1 [redacted] Mathematically IL

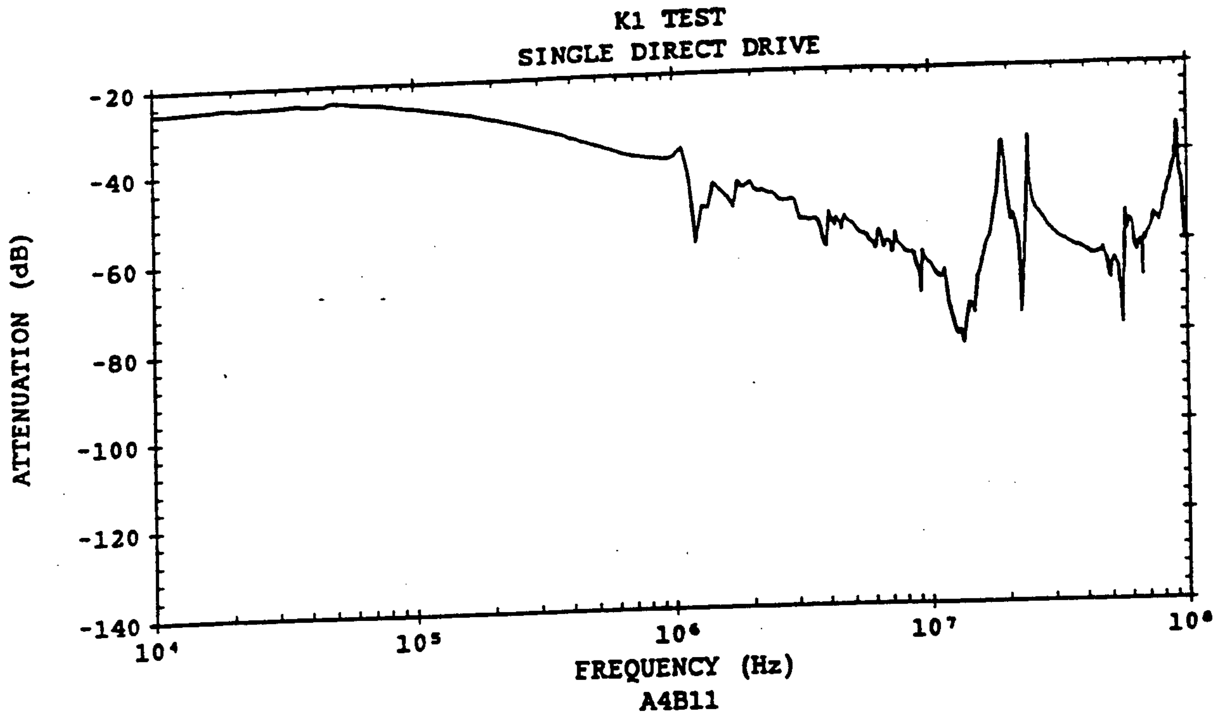

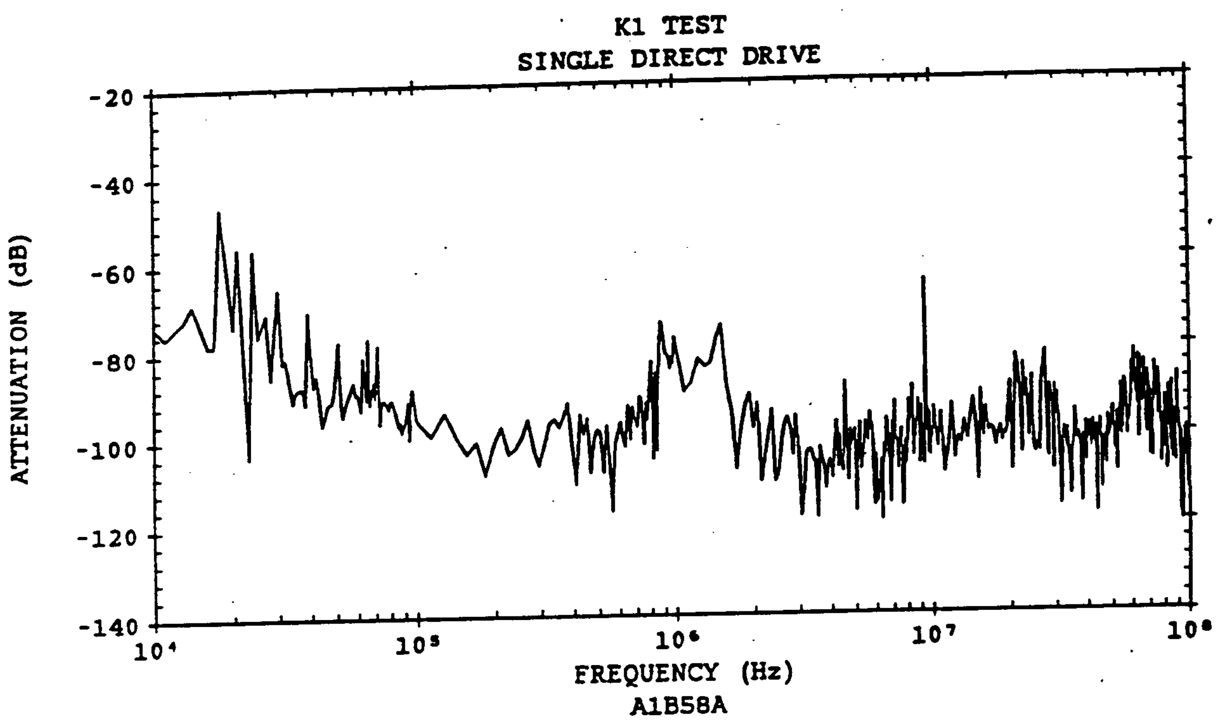

Figure 31. Typical single line direct drive ($|T(f)|$) measurement examples.

is simply a linear average. Physically IL is the amount by which the penetration protection would attenuate a current spike (delta function) on the external cable.

[redacted] Values printed in bold type indicate that the internal test point is hardwire connected [redacted] For example, test points B11 and A4 are the same [redacted] cable, but B11 is inside [redacted] and A4 is outside.

In addition to these hardwire connected test points, a number of cross coupling measurements were performed [redacted]. As expected, [redacted]

3.1.2 [redacted]

Most, but not all [redacted] shield currents are shunted to ground at the penetration panel. Therefore part of the [redacted] currents are conducted to internal equipment. This part is the land line drive [redacted]

To determine the land line drive, the direct drive measurements must be scaled to the actual currents induced on the [redacted] cables in the illumination test. Thus the land line drive (LLD(TP)) at an internal test point [redacted] is given by:

$$LLD(TP) = \Sigma_{\substack{i=1 \\ i \neq 9}}^{10} \left(\frac{TP}{Ai}\right)_{SDD} \cdot \left(\frac{Ai}{H_z(R)}\right)_{ill} \cdot H_z^{thr}(f) \quad (A/Hz) \tag{18}$$

The various entries in expression (18) are defined by equations (16) and (5) in Section 2.1.

Physically equation (18) adds the land line drive contributions from each of [redacted] cables. These contributions are scaled to precisely the actual currents measured on the [redacted] cables in the illumination test (cf. Section 2.2.2.1).

Therefore, the land line drive should theoretically always be smaller than the HEMP stress obtained from the illumination test because it includes land line drive. (Exceptions could occur if the direct drive test somehow excited different coupling paths not driven in the illumination, but this does not apply here.) The difference between the HEMP stress and the land line drive is the local coupling.

Page 57 deleted in its entirety.

Figures 32 to 34 show the land line drive calculated per equation (18) [redacted], compared with the HEMP stresses. Table 7 contains the peak upper bounds for the HEMP stresses and land line drives shown in Figures 32 to 34.

It is evident that the calculated land line drives exceed the HEMP stresses, contrary to expectations. The reason appears to be that the measurements are imperfect: Note that calculation of the land line drive at each test point involves 9 direct drive and 9 illumination measurements, none of them perfect. It is not unreasonable to expect that the cumulative error would amount to the order of 10 dB.

[redacted]

Table 7. [redacted]

3.1.3 [redacted]ILTER INSERTION LOSS

Since [redacted] was not operational, the power filter was accessible for direct drive testing. Figure 35 shows the direct drive measurement [redacted] As mentioned above, this is a low level CW measurement of the attenuation provided by the filter, and does not account for the MOV.

The insertion loss is calculated per equation [redacted]

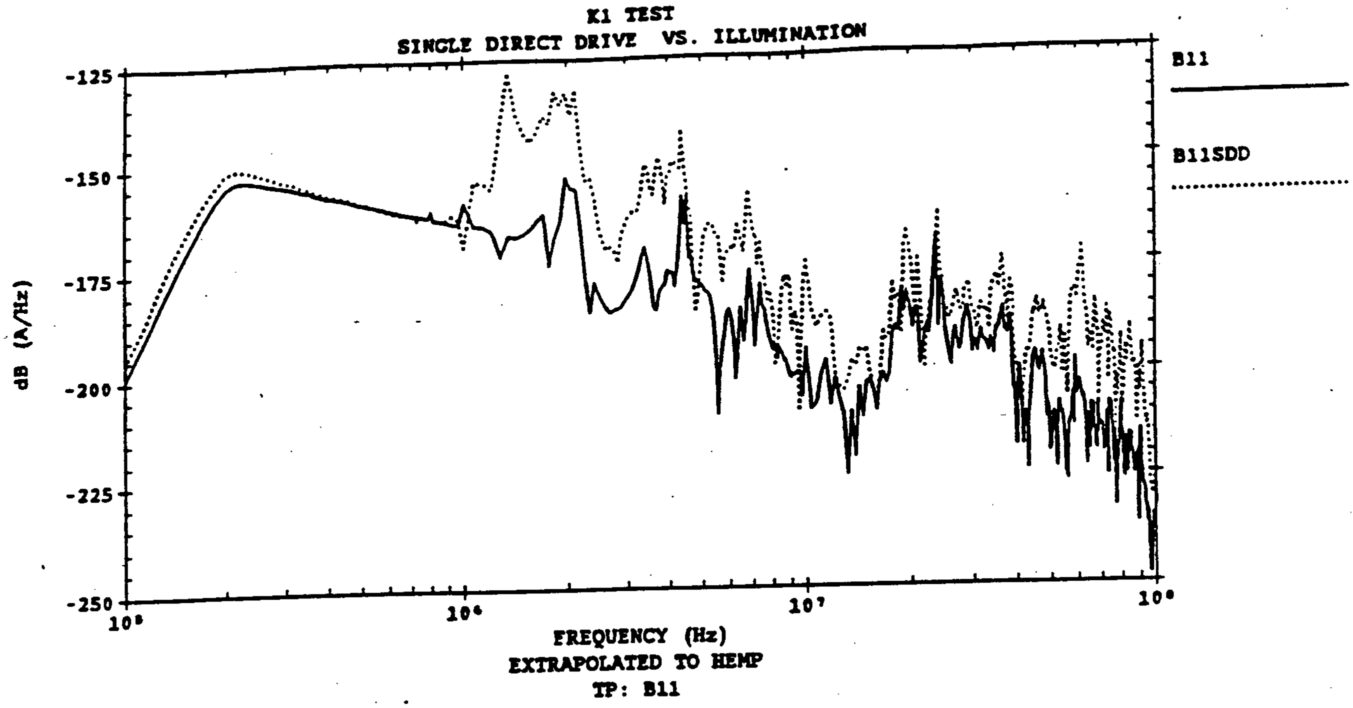

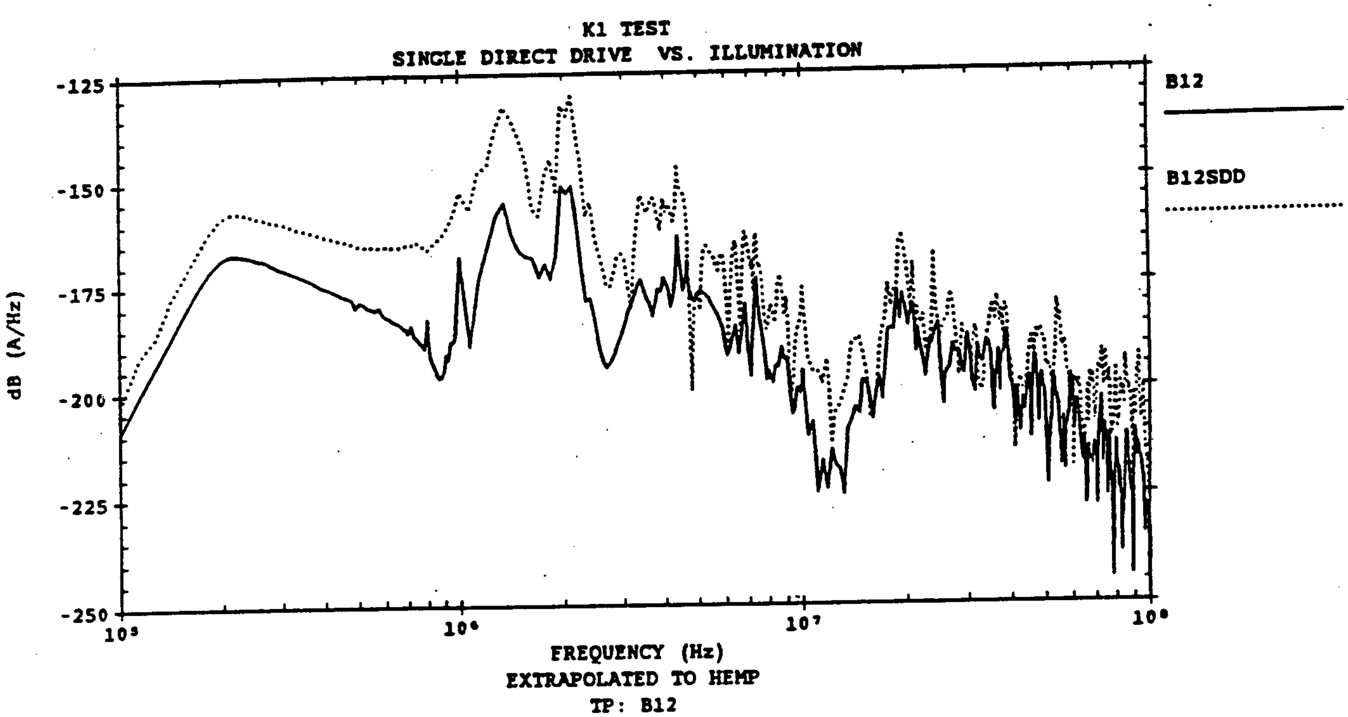

Figure 32. **Land line drive (dotted line) vs. HEMP stress (solid line)** [redacted]

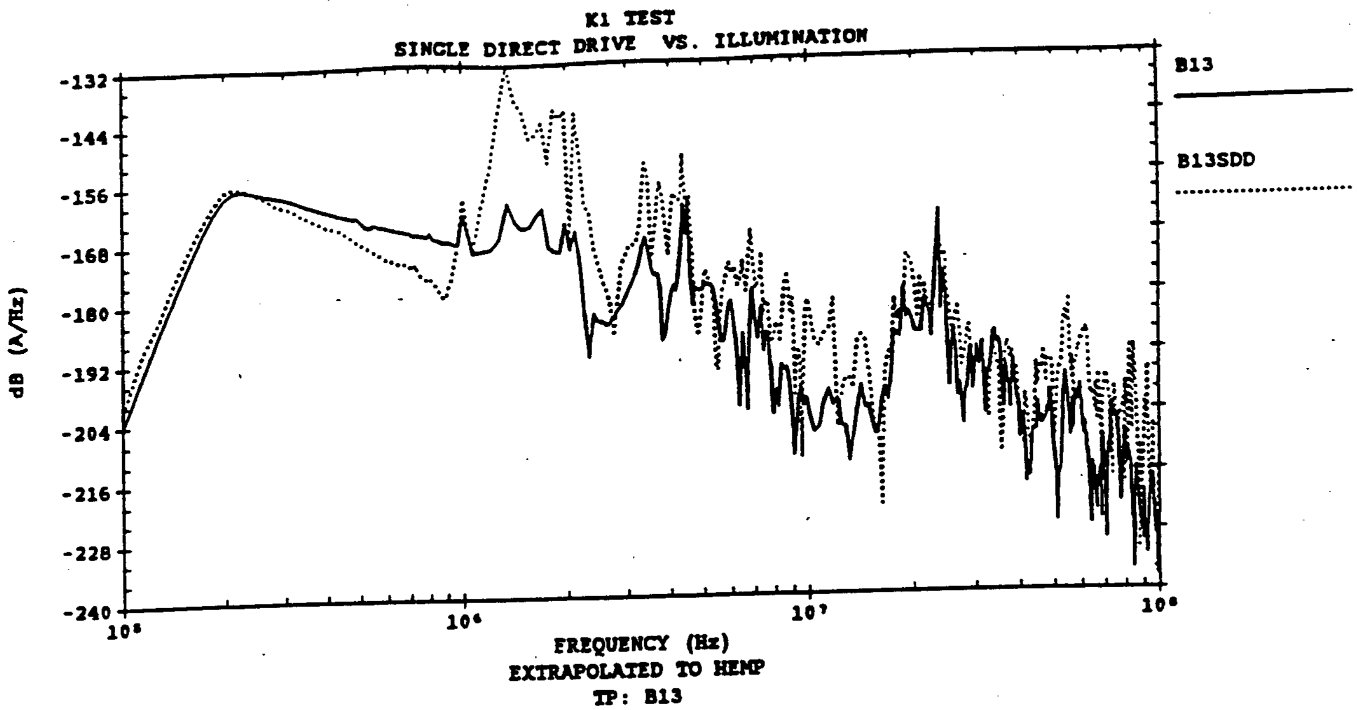

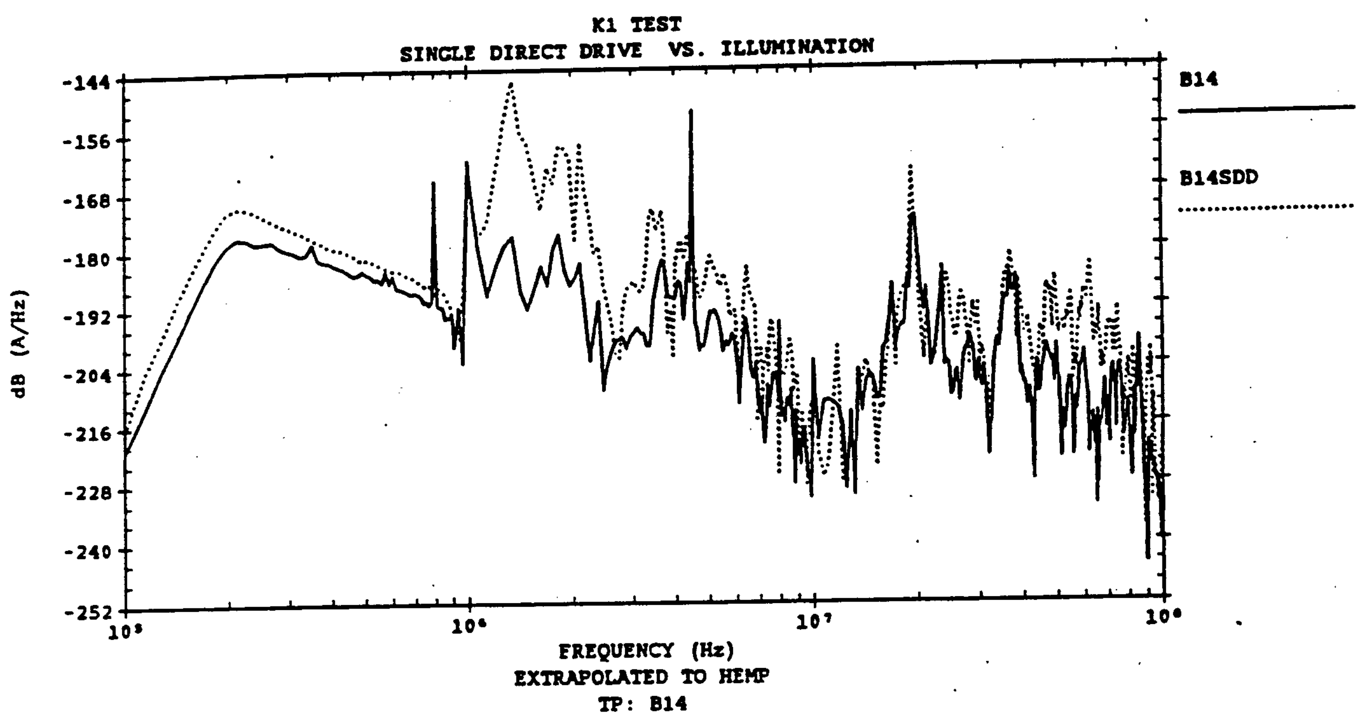

Figure 33. Land line drive (dotted line) vs. HEMP stress (solid line) at [redacted]

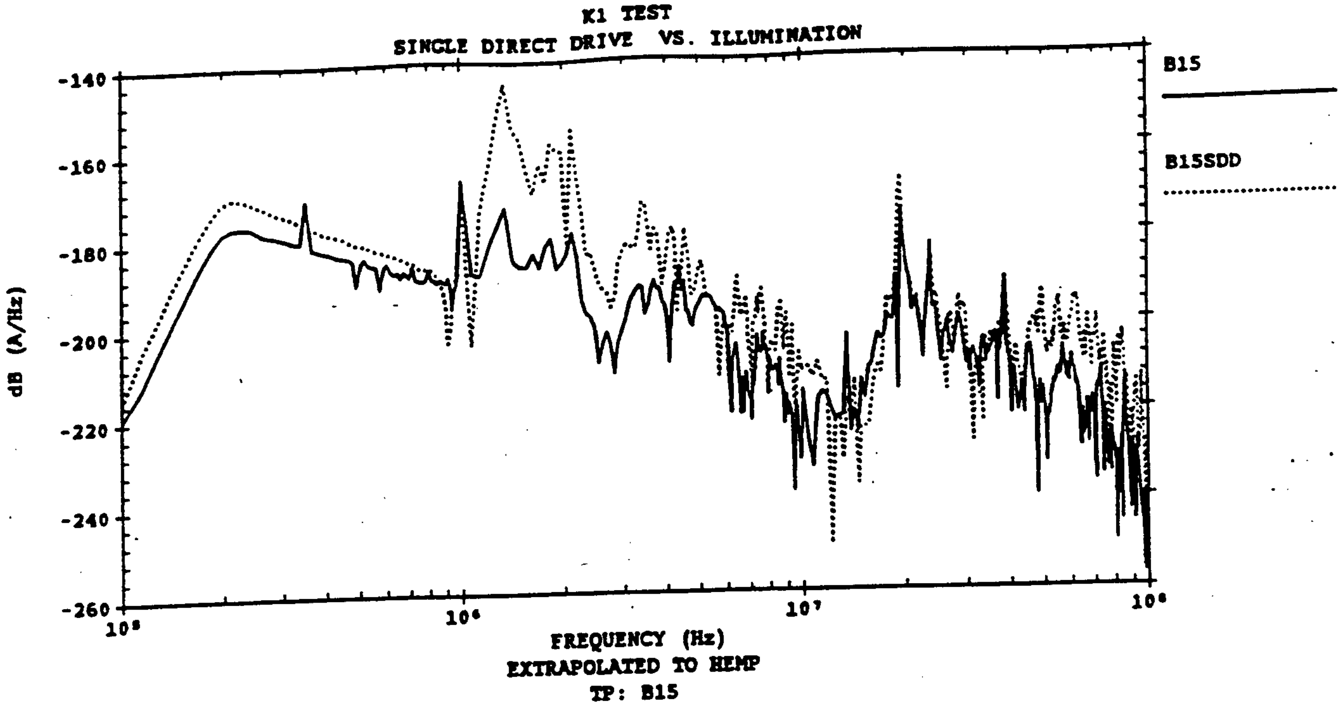

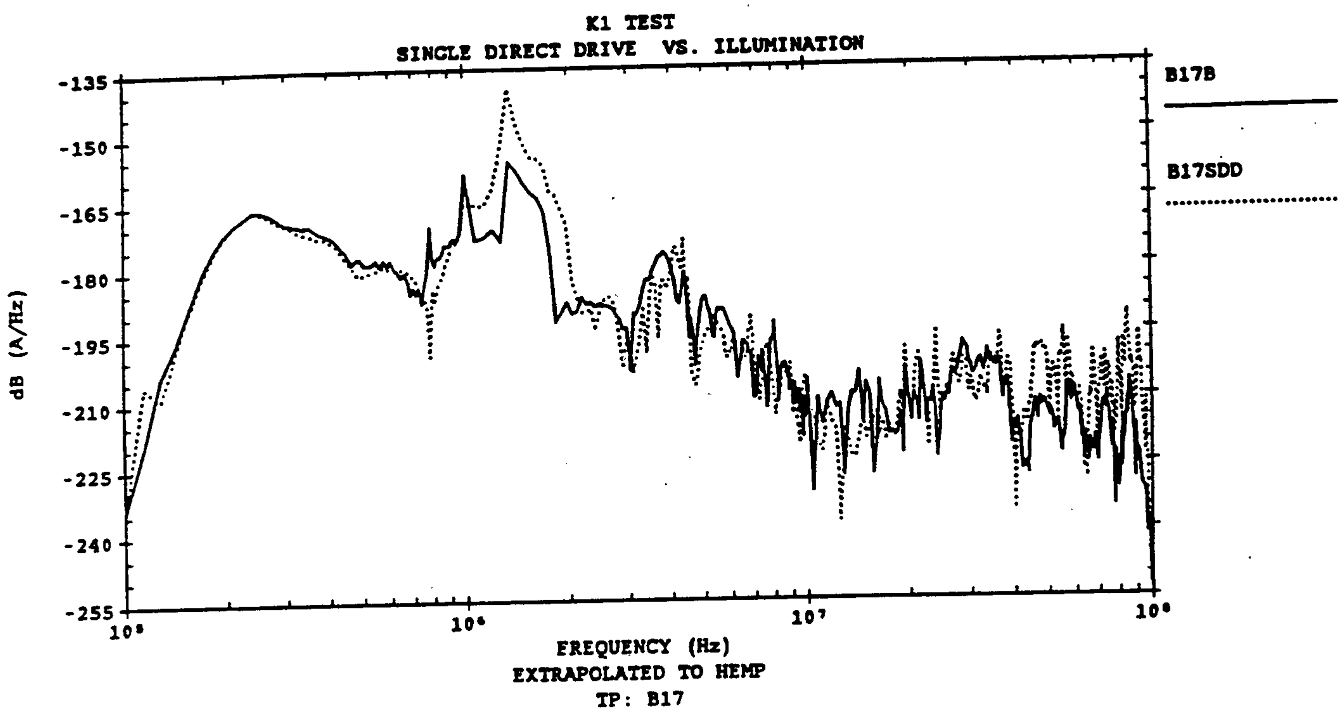

Figure 34. Land line [redacted]P stress (solid line) at [redacted]

[redacted]

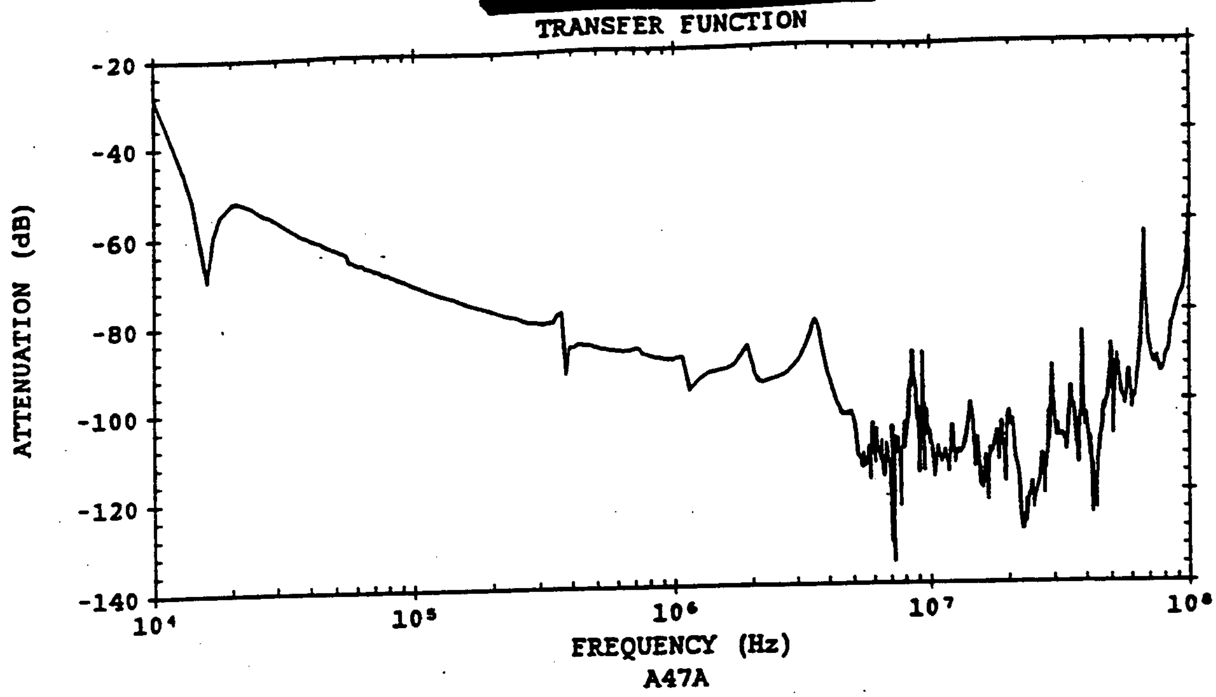

Figure 35. Direct drive measurement [redacted]

3.2 DIRECT DRIVE OF THE TELEPHONE LINE

[redacted] The cable was [redacted] acquired on [redacted] cables inside the building, [redacted]

The insertion loss values calculated per equation (17) are listed in Table 8.

3.3 DIRECT DRIVE OF EER PENETRATIONS

[redacted]

The penetration hardening was evaluated by CW direct driving the cable shields in the [redacted]. Thus the measurements are transfer functions of

Table 8. Insertion loss for telephone line penetration.

[redacted]

the form described in equation (16) from 10 kHz to 100 MHz. These measurements were performed o[redacted]able[redacted] The calculated insertion loss values per equation (17) are listed in Table 9. [redacted]

Table 9. Insertion loss for [redacted]

[redacted]

SECTION 4

CONCLUSIONS

All HEMP stresses [redacted] are less than [redacted] A conservative error bound is 12 dB. These stresses are currents on bundles of shielded and unshielded cables, and on wire bundles. Note that these cable bundles currents are well below the allowed single wire stresses allowed in MIL-STD-188-125. No single wire currents were measured [redacted] because such measurements are impractical at [redacted]

Thus the MIL-STD-188-125 field attenuation requirements can be met despite the fact [redacted] This means that the field attenuation by itself is not a sufficiently sensitive measure of shielding, and that requirements (such as insertion loss) specifically addressing penetration protection effectiveness must augment the field attenuation specification.

The phone line penetration protection works well [redacted]

In addition to the single direct drive tests described in this report, bulk direct drive [redacted] and measurements were acquired [redacted]. Since the bulk direct was conducted on an experimental basis, the analysis and results are documented separately.

All test objectives were met. Lessons learned and recommendations concerning test execution and test equipment improvements were provided in the Test Director's Report (Reference 1).

CHAPTER 5

LIST OF REFERENCES

1. Thomas Zwolinski, "Test Director's Report [redacted] November 1988.

2. Harry Diamond Laboratories, "A Plan for the Validation of the HEMP Hardness [redacted]

3. Wolfgang Bereuter, "Processing of [redacted] Bulk Direct Drive Measurements", to appear.

4. Wolfgang Bereuter and Robert Racca, "HEMP Fields", MRC/COS-M-72, ("unpublished"), 5 December 1988.

5. Wolfgang Bereuter, "Proposed Pass/Fail Criteria for MIL-STD-188-125 CW Immersion Test", MRC/COS-N-TBD, February 1989.

6. Wolfgang Bereuter, "CWMS Testing Threat Relatability", MRC/COS-B-220, 31 October 1986.

7. Wolfgang Bereuter and Robert Racca, "Processing of CWMS Field Map Measurements", MRC/COS-N-131, 9 November 1987.

8. Wolfgang Bereuter, [redacted], to appear.

9. Wolfgang Bereuter et al., [redacted]

10. Wolfgang Bereuter et al., [redacted]

APPENDIX A

HEMP STRESS NORMS

This appendix contains the numerical values for the waveform descriptors or norms PKI, PINT, RIMPI, and RAINT defined below.

$\mathrm{PKI} = \overset{max}{t} \mid i(t) \mid \leq \frac{1}{\pi} \int_{f_0}^{f_1} \mid I(\omega) \mid d\omega = \mathrm{PINT}$	(Amp)	Peak and its upper bound
$\mathrm{RIMPI} = \int_o^T \mid i(t) \mid dt$	(Amp · sec)	Rectified Impulse
$\mid di/dt \mid \leq \frac{1}{\pi} \int_{f_o}^{f_1} \mid \omega I(\omega) \mid d\omega = \mathrm{DIDT}$	(Amp/sec)	Derivative Bound
$\mathrm{RAINT} = \{\frac{1}{\pi} \int_{f_0}^{f_1} \mid I(\omega) \mid^2 d(\omega)\}^{\frac{1}{2}}$	(Amp $\cdot\sqrt{sec}$)	Root Action Integral

$f_0 = 10$ kHz, $f_1 = 100$ MHz, T = 5 μsec.

HEMP STRESS NORMS (continued)

TP	PKI (A)	PINT (A)	RAINT ($A \cdot \sqrt{sec}$)	RIMPI ($A \cdot sec$)	DIDT (A/sec)
[redacted]					
[redacted]					
A1	6.67E+01	1.18E+02	2.76E-02	4.26E-05	1.02E+10
A2	4.86E+01	8.04E+01	1.67E-02	2.76E-05	7.37E+09
A3	2.35E+01	6.65E+01	1.55E-02	2.73E-05	7.24E+09
A4	2.09E+01	5.93E+01	1.12E-02	2.23E-05	7.29E+09
A5	1.30E+01	4.64E+01	8.92E-03	2.01E-05	5.77E+09
A6	2.15E+01	5.92E+01	1.50E-02	2.58E-05	5.06E+09
A7	1.74E+01	4.55E+01	1.03E-02	1.94E-05	4.55E+09
A8	1.95E+01	5.41E+01	9.90E-03	1.74E-05	6.54E+09
A10	2.04E+01	6.38E+01	9.95E-03	1.86E-05	9.23E+09
[redacted]					
A11	4.02E+01	8.57E+01	9.71E-03	1.18E-05	1.52E+10
A12	3.15E+01	6.56E+01	7.41E-03	9.83E-06	1.21E+10
A13	2.90E+01	6.85E+01	9.45E-03	1.19E-05	1.16E+10
A14	1.43E+01	4.33E+01	6.61E-03	1.37E-05	6.87E+09
A15	1.61E+01	4.90E+01	7.34E-03	1.31E-05	8.17E+09
A16	1.71E+01	5.01E+01	6.48E-03	1.00E-05	8.61E+09
A17	8.65E+00	3.26E+01	5.06E-03	9.48E-06	4.87E+09
A18	1.06E+01	4.18E+01	7.45E-03	1.31E-05	6.56E+09
A20	1.57E+01	4.09E+01	5.69E-03	1.04E-05	8.13E+09
[redacted]					
A21	3.24E+01	6.12E+01	5.80E-03	6.55E-06	1.40E+10
A22	4.12E+01	7.97E+01	7.54E-03	7.10E-06	1.85E+10
A23	3.16E+01	6.53E+01	6.84E-03	6.38E-06	1.88E+10
A24	1.59E+01	5.29E+01	6.05E-03	9.40E-06	9.93E+09
A25	1.40E+01	4.65E+01	6.07E-03	8.46E-06	8.81E+09
A26	1.57E+01	5.54E+01	6.51E-03	6.70E-06	1.25E+10
A30	1.32E+01	3.23E+01	3.05E-03	3.15E-06	7.83E+09

HEMP STRESS NORMS (continued)

TP	PKI (A)	PINT (A)	RAINT ($A\cdot\sqrt{sec}$)	RIMPI ($A \cdot sec$)	DIDT (A/sec)
[redacted]					
B11	3.03E-02	7.21E-02	2.23E-05	4.62E-08	4.92E+06
B12	1.61E-02	5.47E-02	1.94E-05	3.38E-08	4.52E+06
B13	2.51E-02	6.10E-02	1.52E-05	2.97E-08	5.30E+06
B14	9.37E-03*	2.27E-02	9.58E-06	2.04E-08*	3.27E+06
B15	3.65E-03	1.24E-02	2.82E-06	5.69E-09	1.56E+06
B17	9.73E-03	2.15E-02	1.01E-05	1.77E-08	1.36E+06
B64	1.02E-02*	1.90E-02	3.02E-05	2.80E-08*	1.06E+06
B66	1.61E-02	5.82E-02	2.02E-05	3.35E-08	4.52E+06
B67	2.46E-02	6.22E-02	1.45E-05	2.91E-08	5.85E+06
B68	3.86E-02	8.05E-02	2.35E-05	4.72E-08	6.25E+06
B69	1.07E-03*	4.09E-03	1.48E-06	1.61E-09*	5.64E+05
B70	1.84E-03	4.96E-03	8.53E-07	1.37E-09	9.76E+05
B71	7.51E-04	2.40E-03	5.11E-07	1.17E-09	3.21E+05
B85	1.54E-02	4.11E-02	1.48E-05	3.54E-08	2.54E+06
[redacted]					
B30	4.42E-03	1.27E-02	2.75E-06	8.50E-09	2.09E+06
B31	6.58E-03	1.55E-02	3.69E-06	1.08E-08	2.62E+06
B32	6.49E-03*	2.11E-02	6.72E-06	1.10E-08*	3.54E+06
B33	4.75E-03*	1.34E-02	5.15E-06	3.11E-09*	2.16E+06
B34	3.61E-03	1.16E-02	1.99E-06	2.45E-09	2.60E+06
B36	1.90E-02	3.34E-02	4.51E-06	5.39E-09	1.04E+07
B65	3.14E-02*	3.07E-02	4.70E-05	1.44E-07*	3.67E+06
B72	4.64E-03	1.56E-02	3.10E-06	5.47E-09	2.68E+06
B73	5.01E-03	2.01E-02	2.75E-06	6.37E-09	4.22E+06
B74	4.28E-03	1.67E-02	3.14E-06	8.44E-09	3.44E+06
B75	1.85E-03	3.54E-03	1.18E-06	4.14E-09	9.20E+05
B76	1.84E-04	4.86E-04	6.75E-08	1.19E-10	1.22E+05
B77	2.91E-03	6.43E-03	1.27E-06	1.56E-09	2.03E+06
B86	2.55E-03*	7.99E-03	8.56E-06	6.86E-09*	8.01E+05

HEMP STRESS NORMS (concluded)

TP	PKI (A)	PINT (A)	RAINT $(A \cdot \sqrt{sec})$	RIMPI (A · sec)	DIDT (A/sec)
[redacted]					
[redacted] B49	2.76E-03	8.41E-03	1.19E-06	1.92E-09	1.62E+06
B50	5.72E-03	1.40E-02	3.40E-06	8.55E-09	2.52E+06
B51	8.46E-03*	1.48E-02	6.05E-06	1.76E-08*	2.36E+06
B55	3.58E-03	1.48E-02	2.31E-06	5.38E-09	2.60E+06
B62	5.87E-02	1.27E-01	1.47E-05	1.34E-08	3.28E+07
B63	2.46E-02	5.74E-02	7.75E-06	1.01E-08	1.80E+07
B78	7.73E-03	1.61E-02	2.95E-06	4.72E-09	3.64E+06
B79	6.41E-03*	1.85E-02	6.07E-06	3.63E-09*	3.38E+06
B80	4.55E-03	1.32E-02	1.62E-06	2.63E-09	2.70E+06
B81	2.45E-03*	6.46E-03	4.63E-06	6.67E-09*	1.50E+06
B82	7.36E-04*	1.67E-03	5.43E-07	1.18E-09*	3.37E+05
B83	5.08E-03	8.38E-03	3.32E-06	1.12E-08	2.03E+06
B84	3.12E-03*	6.21E-03	3.45E-06	1.06E-08*	1.08E+06
[redacted] G3	1.91E-02	4.98E-02	7.59E-06	9.25E-09	2.22E+07
G8	3.42E-02*	2.25E-02	3.95E-05	1.41E-07*	1.84E+06
G9	4.51E-03*	1.13E-02	4.77E-06	1.35E-08*	2.88E+06
G10	8.61E-03*	1.06E-02	1.05E-05	3.60E-08*	2.30E+06
G11	1.15E-03*	2.98E-03	1.35E-06	1.51E-09*	7.99E+05
G12	6.40E-03*	1.21E-02	6.55E-06	1.94E-08*	1.97E+06
G13	4.07E-03	1.22E-02	2.64E-06	6.35E-09	3.14E+06
G14	9.54E-02*	4.83E-02	1.36E-04	4.62E-07*	2.47E+06
G15	7.63E-03*	1.32E-02	1.63E-05	2.97E-08*	2.36E+06
G16	6.67E-03*	1.60E-02	4.91E-06	1.59E-08*	4.25E+06
G17	1.03E-02*	2.37E-02	1.58E-05	3.45E-08*	3.90E+06
G18	1.18E-02	2.58E-02	6.93E-06	2.07E-08	6.40E+06
G19	1.03E-02*	1.95E-02	9.01E-06	2.65E-08*	3.49E+06
G20	5.87E-03*	1.34E-02	5.17E-06	1.50E-08*	2.29E+06
G21	4.17E-03*	9.98E-03	3.88E-06	1.16E-08*	1.60E+06
G31	1.68E-02	4.13E-02	8.82E-06	1.10E-08	1.41E+07
G32	1.65E-02*	2.97E-02	1.24E-05	4.11E-08*	8.77E+06
G33	1.32E-02*	1.84E-02	1.68E-05	4.45E-08*	1.69E+06
G34	1.10E-02*	1.24E-02	1.32E-05	4.50E-08*	2.53E+06
[redacted] W100	2.30E-03*	2.87E-03	5.89E-06	1.05E-08*	1.04E+05
W101	1.86E-03*	1.79E-03	1.63E-06	5.26E-09*	1.08E+05

* = POOR FOURIER INVERSE TRANSFORM (FTE > .3)